

ABSTRACT

Remote sensing and surveillance are the main application areas for radar in general and synthetic aperture radar (SAR) in particular. Since the first radar system built by Hülsmeyer in 1904, radar has developed so that it is now able to create images from a large distance. In addition to this, the invention of SAR has enabled the ability to create images with high resolution. In this thesis, SAR systems capable of very high resolution imaging are considered, and data from such a system, namely CARABAS-II, is used. The higher the resolution of the system, the better the ability to extract information.

The work presented in this thesis can be divided into two separate fields. The first and main area is speed estimation and the refocusing of moving targets in SAR imagery. The second area is related to SAR processing.

In Part I of this thesis, a theoretical expression for the phase of a moving object in a SAR image is derived. Based on this expression, an estimator of relative speed is proposed. The estimator was tested

in simulation and on CARABAS-II data, using a boat as a moving target. The results with regard to the focusing ability were satisfactory. In Part II, a comparison between two high resolution SAR processing algorithms, namely the polar and the subimage version of fast factorized back projection, is made. The comparison takes into account the difference in ability of obtaining very high quality images and gives a phase error analysis. In Part III, the effect of clutter statistics on the estimator is investigated. The sensitivity of the estimator to surrounding stationary targets (coherent clutter) and to thermal noise is examined. The results indicate that a target signal power of approximately 5dB above clutter (peak energy) or noise (average power) gives good results only using one iteration. Part IV is a continuation of Part I and III. In this part, a refocusing approach based on a SAR image is also developed and used. The central part of this refocusing approach is the derivation of a new refocusing equation. The results show that an image with many moving targets that have different normalized relative speeds can be focused.

DEVELOPMENT AND EVALUATION OF SAR ALGORITHMS FOR IMAGE FORMATION AND SPEED ESTIMATION IN WIDEBAND SAR

Thomas Sjögren



ISSN 1650-2140
ISBN 978-91-7295-173-0

Blekinge Institute of Technology
Licentiate Dissertation Series No. 2010:01

School of Engineering



**Development and Evaluation of SAR Algorithms
for Image Formation and Speed Estimation in
Wideband SAR**

Thomas Sjögren



Blekinge Institute of Technology Licentiate Dissertation Series
No 2010:01

**Development and Evaluation of SAR Algorithms
for Image Formation and Speed Estimation in
Wideband SAR**

Thomas Sjögren



Department of Electrical Engineering
School of Engineering
Blekinge Institute of Technology
SWEDEN

© 2010 Thomas Sjögren
Department of Electrical Engineering
School of Engineering
Publisher: Blekinge Institute of Technology
Printed by Printfabriken, Karlskrona, Sweden 2010
ISBN 978-91-7295-173-0
Blekinge Institute of Technology Licentiate Dissertation Series
ISSN 1650-2140
urn:nbn:se:bth-00455

Abstract

Remote sensing and surveillance are the main application areas for radar in general and synthetic aperture radar (SAR) in particular. Since the first radar system built by Hülsmeyer in 1904, radar has developed so that it is now able to create images from a large distance. In addition to this, the invention of SAR has enabled the ability to create images with high resolution. In this thesis, SAR systems capable of very high resolution imaging are considered, and data from such a system, namely CARABAS-II, is used. The higher the resolution of the system, the better the ability to extract information. The work presented in this thesis can be divided into two separate fields. The first and main area is speed estimation and the refocusing of moving targets in SAR imagery. The second area is related to SAR processing.

In Part I of this thesis, a theoretical expression for the phase of a moving object in a SAR image is derived. Based on this expression, an estimator of relative speed is proposed. The estimator was tested in simulation and on CARABAS-II data, using a boat as a moving target. The results with regard to the focusing ability were satisfactory. In Part II, a comparison between two high resolution SAR processing algorithms, namely the polar and the subimage version of fast factorized back projection, is made. The comparison takes into account the difference in ability of obtaining very high quality images and gives a phase error analysis. In Part III, the effect of clutter statistics on the estimator is investigated. The sensitivity of the estimator to surrounding stationary targets (coherent clutter) and to thermal noise is examined. The results indicate that a target signal power of approximately 5dB above clutter (peak energy) or noise (average power) gives good results only using one iteration. Part IV is a continuation of

Part I and III. In this part, a refocusing approach based on a SAR image is also developed and used. The central part of this refocusing approach is the derivation of a new refocusing equation. The results show that an image with many moving targets that have different normalized relative speeds can be focused.

Preface

This licentiate thesis summarizes part of my work within the field of radar signal processing, specifically Synthetic Aperture Radar. The work has been performed at the Department of Electrical Engineering, School of Engineering, at Blekinge Institute of Technology.

The thesis consists of four selected parts:

Part

- I** Speed estimation experiments for ground moving targets in UWB SAR.
- II** A Comparative Study of the Polar Version with the Subimage Version of Fast Factorized Backprojection in UWB SAR.
- III** Moving target relative speed estimation in the presence of strong stationary surrounding using a single antenna UWB SAR system.
- IV** Moving Target Relative Speed Estimation And Refocusing In Synthetic Aperture Radar Images.

Acknowledgments

Throughout this work which has been over 3 years, I have many people to thank. First i would like to thank Dr. Sven Johansson, which accepted me to join the Department of Signal Processing back in 2006. Also a deep thank to my main supervisor, Professor Hans-Jürgen Zepernick which has helped a lot with learning how start writing papers and has also been a good help when it comes to general supervision throughout the making of this thesis. Then i would like to thank my supervisor Dr. Mats Pettersson which has with his rich experience and deep knowledge in SAR system design and signal processing helped a lot with getting into the position. It was Mats that initially gave me the idea of starting this work after having a nice talk in the spring of 2006, as this position was announced on the web of BTH. The whole reason why I came to Ronneby was Lan, my dear friend, why you deserve a special thank. In the everyday work at the department I would like to thank all colleagues in the department for the positive attitude and the open and very friendly style in coffeebreaks, lunches as well as all nice parties. Especially I would like to thank Mikael Swartling for all nice walks in the forest and sessions of board game play. Also I must give a special personal thank for my dear co-Ph.D.-student, Viet which has been a great close colleague in research, coursework as well as very friendly and social to work with.

Most importantly, I would like to give my warm wishes to my parents, Lars and Elisabeth, my sister Erika, my godmother Karin and specially Grosspapi Karl, which has all been a great support throughout my life and given me strength to keep fighting in tough situations. What must not be forgotten as well is all joy that all Tetrinet blocks have given me throughout the years, especially the almighty stick and the wonderful L-block, being

the base for all offensive play in Tetrinet. Last but not least I would like to thank Carlshamn Chamber Choir for all joyful singing moments brought to me during my time in Blekinge so far. It has been challenging, but a weekly boost of joy and energy coming from great friendship and great music.

Ronneby, October 2009 Thomas

List of selected publications

T.K.Sjogren, V.T.Vu and M.I.Pettersson, H-J. Zepernick, A. Gustavsson, *Speed Estimation Experiments for Ground Moving Targets in Low Frequency UWB SAR* In Proceedings for IET International Radar Conference, Edinburgh, UK: 2007.

T.K.Sjogren, V.T.Vu and M.I.Pettersson, *A Comparative Study of the Polar Version with the Subimage Version of Fast Factorized Backprojection in UWB SAR* In Proceedings of International Radar Symposium 2008, Wroclaw, Poland: 2008.

T.K.Sjogren, V.T.Vu and M.I.Pettersson, *Moving Target Relative Speed Estimation in the Presence of Strong Stationary Surrounding Using a Single Antenna UWB SAR System* In Proceedings of IGARSS, Boston, USA: 2008.

T.K.Sjogren, V.T.Vu, M.I.Pettersson, A. Gustavsson, L.M.H. Ulander , *A Method For Moving Target Speed Estimation And Refocusing In SAR* To be Submitted in IEEE Transactions on Aerospace and Electronic Systems.

Contents

Abstract	vii
Preface	ix
Acknowledgments	xi
List of selected publications	xiii
1 Introduction	1
1.1 Radar	1
1.2 Synthetic Aperture Radar	4
1.3 Earth Observation	5
1.4 Surveillance and Security	6
1.5 SAR Processing	7
1.5.1 Global Backprojection	7
1.5.2 Range Migration Algorithm	7
1.6 Moving Objects in SAR	9
1.6.1 Paper I	10
1.6.2 Paper II	10
1.6.3 Paper III	10
1.6.4 Paper IV	10

I Speed estimation experiments for ground moving targets in UWB SAR	13
II A Comparative Study of the Polar Version with the Subimage Version of Fast Factorized Backprojection in UWB SAR	21
III Moving target relative speed estimation in the presence of strong stationary surrounding using a single antenna UWB SAR system	27
IV Moving Target Relative Speed Estimation and Re-focusing in Synthetic Aperture Radar Images	33

Chapter 1

Introduction

The wish for humans to explore nature is the core for the development and survival of the human race. Since the space race began in the 1950s with the launch of Sputnik[1], we have used spacecrafts to explore our planet's closest surroundings. These explorations have given us a better understanding of how dependent we are on the surrounding atmosphere, for instance the ozone layer, and how important it is to supervise it[2]. Radar and especially Synthetic Aperture Radar (SAR) systems are very important for the continuous supervision of the Earth climate[3] and they are also crucial as sensors capable of high-resolution mapping of space bodies[4]. In the introductory part of this thesis, some history and also the basic principles of radar and SAR are given.

1.1 Radar

The main sensors used in remote sensing that create 2-D mappings of the ground are active sensors such as LIDAR and radar or passive sensors such as photometers (standard optical cameras) and radiometers. Out of these four sensors, the radiometer and the radar are the only ones almost independent of weather conditions. The photometer not only depends on good weather, but also on sunlight to illuminate the ground.

The abbreviation radar comes from Radio detection and ranging and the basic principle of radar is to illuminate an object and analyze the received response with the help of electromagnetic (EM) radiation. Based

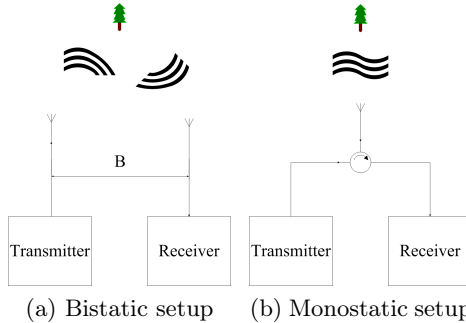


Figure 1.1: Two different configurations of a basic radar system.

on this, the most basic radar system is a bistatic system that consists of a transmitter and a receiver which have one antenna each. However, it is possible for the transmitter and receiver to share an antenna, making the radar system monostatic, which most systems are today. In Figure 1.1 (a) and (b), the bistatic and monostatic radar configurations are shown respectively. Another radar configuration is the multistatic setup that make use of many transmitters and receivers that together form a radar network. In addition to these configurations, it is also possible to use bistatic or multistatic passive radars in which the receivers make use of other transmitters such as a GPS signal, a TV signal or an FM Radio signal.

Radar systems have been used since the beginning of the 20th century. It is often argued that the german inventor Hülsmeyer was the one to introduce radar [8]. His invention was called the telemobiloscope and it used a bistatic configuration. It was placed on the river Rhine for the purpose of detecting ships traveling in fog. The system operated in the UHF band, something that today would lead to radio frequency interference problems from TV broadcasters as well as from GSM communication. The radar was not adopted by civilian or military organisations until the 1930s, when the military realized the usefulness of this technology. Most of the continued development of radar has also been conducted by the military and in Sweden some famous radar systems have been developed, including ERI-EYE, PS-05/A, GIRAFFE, ARTHUR, LORA and CARABAS. Data from CARABAS-II has been used in the work presented in this thesis.

Fully coherent radar needs very precise oscillators. Therefore, the system has very precise knowledge of the transmitted signal and of the position of the transmitter and receiver. Another perspective of radar is that the wave velocity in air is well known and approximately the same as in vacuum. This means that the timing relation to distance is very exact.

The most common type of radar is probably the one that incoherently transmits short pulses. This type of system uses a pulse which has a large energy and a short time. For high-performance systems, it is more common to transmit a wide-band pulse over a long time and after that perform pulse compression. In these pulse radars, it is common to use chirp waveforms. In order to obtain a good range resolution for the radar, the transmitted signal is saved and later convolved with the received signals, something referred to as pulse compression. A standard chirp signal can be written as

$$s_t(\tau) = e^{-i2\pi(\phi_0 + f_c\tau + k\tau^2)}, \tau \in \left[-\frac{T_p}{2}, \frac{T_p}{2}\right] \quad (1.1)$$

where τ is fast-time, ϕ_0 an arbitrary phase, k is the fast time chirp rate, f_c is the center frequency and T_p is the pulse length.

If compensating for the path loss, the received echo signal from an object at the distance R will be

$$s_r(\tau) = e^{-i2\pi\left(\phi_0 + f_c\left(\tau - \frac{2R}{c}\right) + k\left(\tau - \frac{2R}{c}\right)^2\right)}, \tau \in \left[-\frac{T_p}{2} + \tau_d, \frac{T_p}{2} + \tau_d\right] \quad (1.2)$$

After convolving, $s_r(\tau)$, with its matched filter namely $(s_t(-\tau))^*$, where $*$ denotes complex conjugation, the pulse compressed signal $s_{pc}(\tau)$ can be determined. This signal is given by

$$\begin{aligned} s_{pc}(\tau) &= T_p \left(1 - \frac{\left| \frac{2R}{c} - \tau \right|}{T_p} \right) e^{i2\pi\left(\frac{2R}{c} - \tau\right)f_c} \\ &\cdot \text{sinc} \left(2\pi k T_p \left(\frac{2R}{c} - \tau \right) \left(1 - \frac{\left| \frac{2R}{c} - \tau \right|}{T_p} \right) \right), \tau \in \left[\frac{2R}{c} - T_p, \frac{2R}{c} + T_p \right] \end{aligned} \quad (1.3)$$

The windowed *sinc* function has a much better resolution in range compared to $s_r(\tau)$. We say that we have compressed the signal energy to a short time duration. The way to obtain good resolution in elevation and azimuth for a radar is by creating very narrow beams.

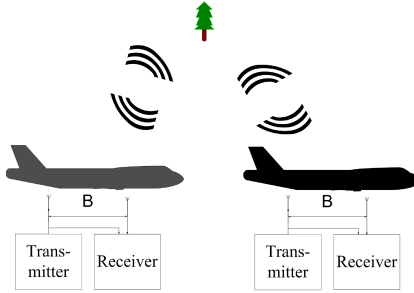


Figure 1.2: Standard setup for a 2-channel along track SAR system used for moving target detection, having the baseline of length B.

1.2 Synthetic Aperture Radar

In 1951, Wiley discovered that it was possible to obtain a resolution better than that provided by the antenna beam. He discovered that the motion of the platform can be used to obtain a resolution much finer than the size of the antenna footprint and in 1965, he filed the patent named "Pulsed Doppler Radar Methods And Apparatus" [9]. In these first SAR systems, the resolution was greatly improved compared to real aperture radar. Since then, the development has continued and the system today with the best resolution with respect to wavelength is the CARABAS-II system that has a resolution lower than the shortest wavelength of the system.

In SAR systems as well as in traditional radar, both monostatic and bistatic configurations are possible. In Figure 1.2, a standard SAR setup for the imaging of moving targets is shown. The two antennas alternate as transmitters and both antennas are connected to the receiver. In the following derivations of this section, a monostatic SAR system is assumed.

The basic principle of SAR is the collection of radar echoes from a hypothetical stationary target as the SAR system moves along a straight flight track, called the synthetic aperture. The longer the synthetic aperture is, the larger the so called integration angle will be, which is the quantity that decides the resolution of the system. The fact that the resolution is a function of integration angle only makes the resolution independent of the distance from the scene. This can be contrasted with optical sensors that are limited by the resolution in the viewing angle.

In the same way as for radar, the important thing is the signal after pulse compression. As the SAR platform moves along a hypothetical straight flight track, the radar emits and receives pulses. Considering one object of interest, the difference between pulses will be determined by the attenuation of the signal from the path loss and the antenna pattern as well as by the change in distance to the object. Based on this, the pulse-compressed signal before SAR processing is

$$s_{pc}(\tau, t) = T_p \left(1 - \frac{\left| \frac{2R(t)}{c} - \tau \right|}{T_p} \right) e^{i2\pi \left(\frac{2R(t)}{c} - \tau \right) f_c} \cdot \text{sinc} \left(2\pi k T_p \left(\frac{2R(t)}{c} - \tau \right) \left(1 - \frac{\left| \frac{2R(t)}{c} - \tau \right|}{T_p} \right) \right), \tau \in \left[\frac{2R(t)}{c} - T_p, \frac{2R(t)}{c} + T_p \right] \quad (1.4)$$

where the range to a target is a function of t , so-called slowtime, and is given by $R(t) = \sqrt{(X - v_{pit}t)^2 + Y^2}$. Here, X and Y is the azimuth and slant-range position of the object. Slowtime is the azimuth time vector, which relates to the movement of the SAR platform during illumination of the scene of interest. Based on this pulse-compressed data, many algorithms that are able to obtain a SAR image have been proposed. Among the more accurate algorithms, usable even in relation to large integration angles, Range Migration(RMA)[5] and Global Backprojection(GBP)[6] should be mentioned. Consequently, their basic functions are presented later in the introduction.

1.3 Earth Observation

Space-based earth observation began with the rocket development that had its first major breakthrough with the V2 rocket developed by Wernher von Braun. Since the Sputnik, which in 1957 became the first spacecraft to orbit the Earth[1], a large number of spacecrafts have circled the globe. Early measurements of the atmosphere focused on temperature and radiation. Phenomena such as the Aurora Borealis was of interest during in the beginning of the exploration of space. Esrange in Sweden was established in 1966 for the study of the Aurora Borealis and the first Rocket experiments where made the same year. These are also the first Swedish

in situ measurements from space. Later on, as more scientific satellites were launched, instruments that mapped the Earth's surface were able to make topographic maps, classify land, sea, forest and cultivated lands. In addition to this, they were able to help out during natural catastrophes such as earthquakes and man-made disasters such as oil spills. Among Swedish Earth observation satellites, Odin should be mentioned. From an Earth Observation point of view, this is a very interesting satellite as it gives information about the amount of ozone in the ozone layer. Important European Space Agency (ESA) Earth observation satellites include ERS-I, ERS-II and ENVISAT, all having a SAR system as an important instrument on board. Recently launched and highly important satellites are TerraSAR-X and Tandem-X, which are two German SAR-satellites, as well as the Italian Cosmos-Skymed which will have a system of 4 SAR-satellites. The last mentioned projects are combined civilian and military satellites which also have modes of operation able to detect moving targets. It should also be mentioned that the first of the coming set of 5 different ESA SENTINEL satellite missions is a SAR satellite mission. This shows how greatly ESA values SAR systems in space.

1.4 Surveillance and Security

As already mentioned, SAR has some specific advantages in regard to operation in darkness and in bad weather conditions. Important is also the high precision oscillator that forms pulses that are almost exactly known in time and that the position of the SAR platform for each pulse is known with high accuracy. Since the SAR image is a coherent combination of all pulse echoes, the sensitivity for change between two images in a SAR scene is high. The decorrelation between measurements is mainly driven by clutter statistics. This fact has been used in so called coherent change detection[7], where the same scene is imaged two times during two flights with an aircraft or during two passes by a satellite. If instead two or more receivers are mounted on the same platform, displaced along the flight direction, a small time difference between the two SAR images is obtained. This creates the ability to detect movement in an image. In this case, the decorrelation of the clutter will be very low. In surveillance of, for instance, land or sea, the use of formation flying satellites, using a

high pass filter in time - also known as MTI filtering - makes it possible to detect moving targets.

1.5 SAR Processing

As with traditional radar, the first step in many SAR processing algorithms is pulse compression. After this, the SAR image is formed using either processing in the 2D frequency domain or in the 2D spatial domain. In connection to this thesis, many algorithms have been implemented. However, only two basic algorithms will be explained here. In this section, a spatial domain algorithm, namely GBP will first be presented, followed by a frequency domain algorithm named RMA.

1.5.1 Global Backprojection

In Global Backprojection (GBP), the SAR image is formed by evaluating the GBP integral, which is given by

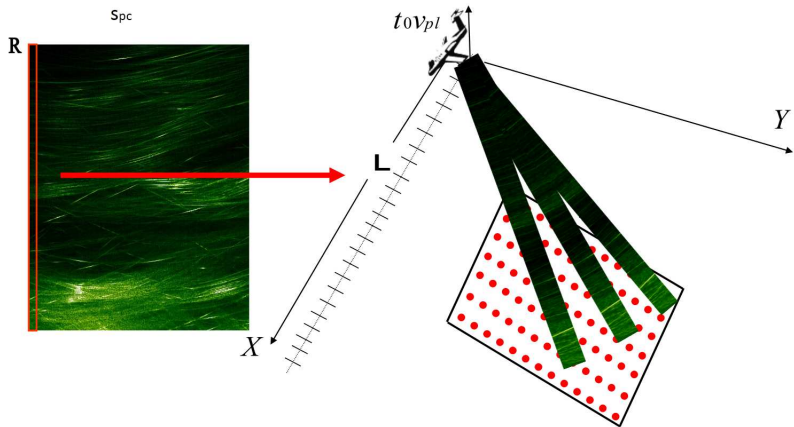
$$h(X, Y) = \int_{-\infty}^{\infty} s_{pc}(\tau, t) dt \quad (1.5)$$

For each pixel position, (X, Y) in the SAR image, a coherent summation of the radar echoes over all slowtime positions is carried out. In Figure 1.3 a the procedure of GBP is illustrated. In Figure 1.3 b-d, SAR images generated using GBP with an increasing part of the aperture are shown.

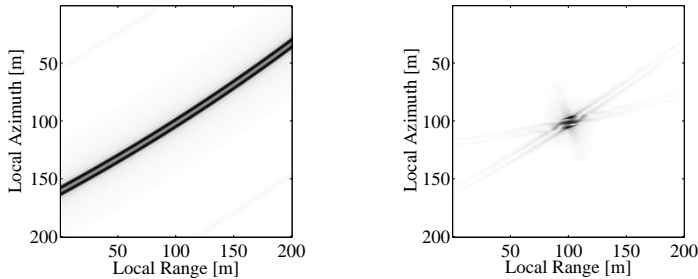
1.5.2 Range Migration Algorithm

When using the Range Migration Algorithm (RMA), the idea is to do the processing in the 2D frequency domain, also known as the 2D wave-domain. The main step in RMA is a change of variables in the 2D wave domain, $k_\rho = \sqrt{k_R^2 - k_x^2}$, where k_ρ is the wavenumber in slant range, k_x is the azimuth wavenumber and k_R is the wavenumber in pulse compressed raw data. After this, the signal is multiplied with two functions and transformed back to the spatial domain, giving a SAR image. The first function, which is a pure magnitude function, is

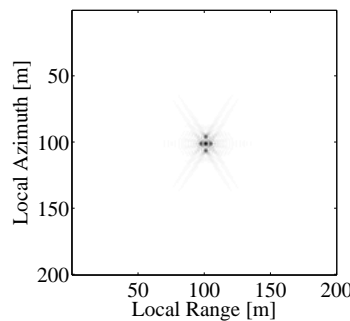
$$S_1 = k_\rho / \sqrt{k_x^2 + k_\rho^2} \quad (1.6)$$



(a) Illustration of Global Backprojection. To the left, the SAR data after pulse compression is shown. To the right, the process of backprojecting this data onto the image is illustrated.



(b) GBP image using one pulse. (c) GBP image using one third of the aperture, which in this specific case is 2390 aperture positions.



(d) GBP image using the complete aperture.

Figure 1.3: SAR image formation using Global Backprojection(GBP) consists of the backprojection of the pulse-compressed data onto the image grid in a pulse by pulse manner.

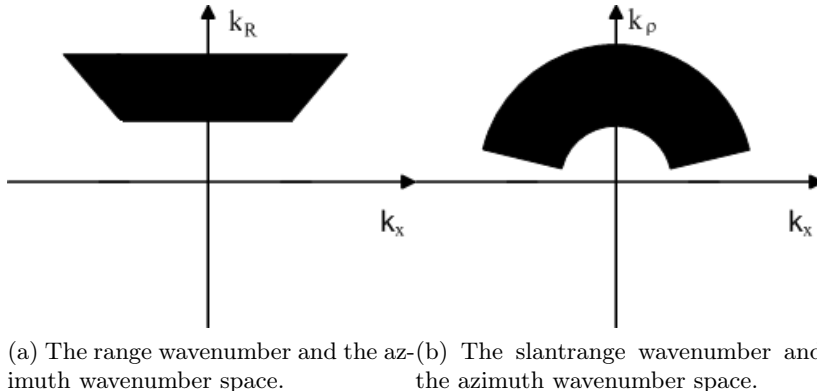


Figure 1.4: SAR image formation using the Range Migration Algorithm (RMA) consists essentially of the transformation from a to b.

while the second one, which is a pure phase function, is

$$S_2 = e^{-j(r_c \sqrt{k_x^2 + k_p^2} - k_p)} \quad (1.7)$$

1.6 Moving Objects in SAR

In a SAR image, a moving object typically effects the image negatively in two ways, namely through defocusing and by shifting its position. Another effect that moving objects cause in SAR images is that the phase information is changed. This fact is utilized in this thesis. A typical effect produced by moving objects in SAR imagery is the one produced by trains when imaged by spaceborne SAR systems. Here, the train appears to move parallel to the train track. With very high resolution SAR, such as UWB SAR, that makes use of long integration times, the moving target will have its energy spread out in a curved shape, either as a parabola or a hyperbola. The papers in this thesis focus on moving objects and their effects on SAR images.

1.6.1 Paper I

The main contributions in Paper I are the derivation of an expression for the phase in a SAR image as a function of target normalized relative speed (NRS). This paper also proposes an iterative method for estimating the NRS of a moving target in a SAR image and it presents successful results from a simulation as well as from using CARABAS-II data.

1.6.2 Paper II

In paper II, the main contribution is a comparative study between two SAR processing algorithms suitable for UWB SAR processing, namely two versions of Factorized Fast Backprojection. The outcomes were that one version appears faster, while the other is capable of higher accuracy imaging.

1.6.3 Paper III

In Paper II, the work begun in Paper I was further investigated using simulations of how the estimation approach is affected at different levels of simulated clutter and noise. This paper also investigates whether the covariance matrix, that was based on an estimation of the clutter covariance matrix, is capable of improving the estimates.

1.6.4 Paper IV

Paper I and Paper III are the bases for Paper IV. However, in this paper, the formula from Paper I is more generally derived. Also, a new equation based on the Range Migration Algorithm is derived which allows for refocusing. The refocusing is shown to work on a simulated target inserted in a CARABAS-II scene as well as on a simulated scene.

Bibliography

- [1] W.J. Jorden, "Soviet Fires First Satellite Into Space," The New York Times, 1957.
- [2] J.C. Farman, B.G. Gardiner and J.D. Shanklin, "Large losses of total ozone in Antarctica reveal seasonal ClO_x/NO_x interaction," Nature, vol. 315, no. 6016, pp. 207-210, 1985.
- [3] J.F. Vesecky, R.H. Stewart, "The observation of ocean surface phenomena using imagery from the SEASAT synthetic aperture radar: An assessment," Journal of Geophysical Research, vol. 87-5, pp. 3397-3430, 1982.
- [4] E. R. Stofan et al, "The lakes of Titan," Nature, vol. 445, no. 7123, pp. 61-64, 2007.
- [5] C. Cafforio, C. Prati, and F. Rocca, "SAR Data Focusing Using Seismic Migration Techniques," IEEE Transactions on Aerospace and Electronic Systems, vol. 27, no. 2, pp. 194-207, 1991.
- [6] L.E. Andersson, *On the Determination of a Function From Spherical Averages* SIAM Journal on Mathematical Analysis, vol. 19, no. 1, pp. 214-232, 1988.
- [7] L. M. H. Ulander, M. Lundberg, W. Pierson, and A. Gustavsson, *Change detection for low-frequency SAR ground surveillance* IEE Proceedings on Radar Sonar and Navigation, vol. 152, no. 6, pp. 413-420, 2005.

- [8] C. Hülsmeyer, "Verfahren, um entfernte metallische Gegenstände mittels elektrischer Wellen einem Beobachter zu melden," Kaiserliches Patentamt, Patent nr 165546, 1904.
- [9] G. Franceschetti, R. Lanari, "Synthetic Aperture Radar Processing," CRC Press, 1999.

Part I

Speed estimation experiments for ground moving targets in UWB SAR

SPEED ESTIMATION EXPERIMENTS FOR GROUND MOVING TARGETS IN UWB SAR

T. K. Sjögren*, V. T. Vu*, M. I. Pettersson*, H.-J. Zepernick*, A. Gustavsson†

* Blekinge Institute of Technology, Department of Signal Processing

P.O. Box 520, SE-372 25 Ronneby, Sweden

E-mail: thomas.sjogren@bth.se, Fax +46 457 27914, Phone +46 733 38 47 88

† Swedish Defence Research Agency, Department of Radar Systems

P.O. Box 1165, SE-581 11 Linköping, Sweden

Keywords: SAR, UWB, speed estimation, focusing, normalised relative speed.

Abstract

This paper presents an iterative method to estimate the Normalised Relative Speed (NRS) of ground moving targets in Ultra Wideband (UWB) wide beam Synthetic Aperture Radar (SAR) using one antenna. The number of iterations depends on the separation between processed NRS and true target NRS. The NRS estimate is based on a chirp rate estimator in azimuth direction of the SAR image. The paper derives an analytical expression of the azimuth phase information based on the moving target NRS and the NRS used in the image formation. The method has been tested on real data from the CARABAS-II SAR system showing good results.

1 Introduction

One of the challenges in wideband Synthetic Aperture Radar (SAR) processing relates to defocusing and displacement of moving targets. These effects are more severe in Ultra Wideband (UWB) systems with large antenna beamwidth connected to long integration time. The amount of displacement and smearing depends not only on the integration time, but also on the Normalised Relative Speed (NRS) of the moving target. Assuming no accelerations, a focused moving target can be obtained using the NRS [6]. Depending on the dynamics of the target, the linear speed model will be limited in time due to accelerations. Investigations on speed estimation errors due to the influence of accelerations have been carried out in [9].

To suppress clutter and to estimate speed, one typically uses methods like Displaced Phase Centre Antenna (DPCA), Space Time Adaptive Processing (STAP) and Along-Track Integration. A useful method for estimating the speed is based on filter banks [5], which applies a filter to the SAR image for a set of speeds where the strongest amplitude response in the image corresponds to the most likely speed. In [6], the usage of an antenna array to suppress clutter was explained. In [2], an estimator of

relative speed for narrow band SAR was suggested. Another method to obtain speed information from a SAR image is presented in [7], where the speed of a target, or even the full velocity vector, can be estimated using knowledge of the antenna pattern.

Most published work regarding speed estimation is on narrow beam SAR systems but not much attention has been given to wide beam applications. In addition, to our knowledge there are not many publications in the field of low frequency systems. In this paper, an iterative NRS estimation method is presented and tested successfully on real data from UWB SAR system that operates in the Very High Frequency (VHF) band. The derived method has the advantage of fast convergence into a good estimate and the ability to estimate the NRS even when the target is surrounded by a number of strong stationary targets. This is due to the fact that the phase of the stationary targets is negligible outside their extent, while the phase of the moving target is spread over a larger area in the image. The method is mainly limited by two assumptions that must hold, i.e. the moving target has been detected and the minimum range to the target is known. A third assumption is made that the target moves with constant NRS, which will affect the quality of the estimate.

In Section 2, the phase of an unfocused target in azimuth direction is derived. In Section 3, we present the estimator for NRS used in the proposed method. In Section 4, experimental results using simulations as well as results on real data are presented. In Section 5, we summarise our work.

2 Phase of unfocused moving target in azimuth direction

The range from the SAR sensor to an arbitrary point on the ground can be formulated as

$$r(\xi, \eta, t) = \sqrt{(v_{pl}t - \xi)^2 + \eta^2 + h^2} \quad (1)$$

where ξ and η are the ground coordinates in the along-track direction and the cross-track direction, respectively, h is the flight altitude of the sensor, t is time and v_{pl} is the

speed of the SAR platform. Let X_t and Y_t denote the coordinates of a focused target with the NRS γ_t . As described in [8], the true range from the sensor to a moving target is

$$r_t(t) = \sqrt{\gamma_t^2(v_{pl}t - X_t)^2 + Y_t^2} \quad (2)$$

where the NRS γ_t , which depends on target speed in along-track v_ξ and cross-track v_η , is defined as

$$\gamma_t = \sqrt{\frac{(v_{pl} - v_\xi)^2 + v_\eta^2}{v_{pl}^2}} \quad (3)$$

Let X_p and Y_p denote image coordinates for a SAR image processed at the NRS γ_p . The range from the sensor to an arbitrary image coordinate is

$$r_p(X_p, Y_p, t) = \sqrt{\gamma_p^2(v_{pl}t - X_p)^2 + Y_p^2} \quad (4)$$

Figure 1 illustrates a typical curve in SAR images caused by a moving target. The minimum range is found at the coordinates (X_t, Y_t) .

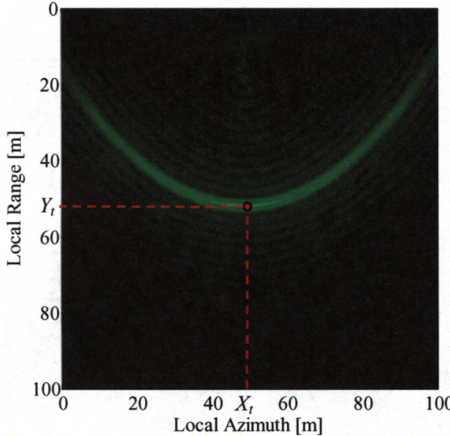


Figure 1. Illustration of a moving target in a SAR image.

If the processed NRS γ_p is equal to the true NRS γ_t , the moving target will be focused at the point (X_t, Y_t) . If we assume that the transmitted waveform from the radar system is a chirp pulse, the SAR image coordinate point (X_p, Y_p) can be found from the Global Backprojection (GBP) [1] integral

$$h(X_p, Y_p) = \int_{-\infty}^{\infty} e^{\frac{-j4\pi f_c \partial r(X_p, Y_p, t)}{c}} \text{sinc}\left(\frac{2\pi B \partial r(X_p, Y_p, t)}{c}\right) dt \quad (5)$$

where the range error is defined as

$$\partial r(X_p, Y_p, t) = r_t(t) - r_p(X_p, Y_p, t) \quad (6)$$

and B is the bandwidth of the signal, f_c is the centre frequency, and c is the speed of light.

Under the assumption of stationary phase [3], the integral in Equation (5) can be approximated as

$$h(X_p, Y_p) \approx e^{\frac{-j4\pi f_c \partial r(X_p, Y_p, t_{st})}{c}} \text{sinc}\left(\frac{2\pi B \partial r(X_p, Y_p, t_{st})}{c}\right) \quad (7)$$

where t_{st} is the time of stationary phase of the target.

The smallest range error, which corresponds to the time of stationary phase t_{st} , is obtained when the derivative of Equation (6) is equal to zero, that is

$$\frac{v_p \gamma_t^2 \cdot (v_{pl} t_{st} - X_t)}{r_t(t_{st})} - \frac{v_{pl} \gamma_p^2 \cdot (v_{pl} t_{st} - X_p)}{r_p(X_p, Y_p, t_{st})} = 0 \quad (8)$$

Furthermore, we make the assumption that

$$r_t(t_{st}) \approx r_p(X_p, Y_p, t_{st}) \quad (9)$$

The approximation in Equation (9) can be motivated by the sinc factor in the integral of Equation (5). The main contribution to the integral will be found within the first zeros of the sinc function. Since typically

$$r_t(t_{st}) \gg \frac{c}{2B} \quad (10)$$

the assumption in Equation (9) is justified. Thus, t_{st} can be found from

$$\frac{v_p \gamma_t^2 \cdot (v_{pl} t_{st} - X_t) - v_{pl} \gamma_p^2 \cdot (v_{pl} t_{st} - X_p)}{r_t(t_{st})} = 0 \quad (11)$$

or

$$t_{st} = \frac{X_t \gamma_t^2 - X_p \gamma_p^2}{v_{pl} \cdot (\gamma_t^2 - \gamma_p^2)} \quad (12)$$

Applying the law of conjugates, Equation (6) can be rewritten at the time of stationary phase of the target t_{st} as

$$\partial r(X_p, Y_p, t_{st}) = \frac{\gamma_t^2 \cdot (v_{pl} t_{st} - X_t)^2 + Y_t^2 - \gamma_p^2 \cdot (v_{pl} t_{st} - X_p)^2 - Y_p^2}{r_t(t_{st}) + r_p(X_p, Y_p, t_{st})} \quad (13)$$

and can be approximated as

$$\partial r(X_p, Y_p, t_{st}) \approx \frac{\gamma_t^2 \gamma_p^2 (X_t - X_p)^2 + Y_t^2 - Y_p^2}{2r_t(t_{st})} \quad (14)$$

From Equation (14), we can write the phase given in Equation (7) as

$$\Phi(X_t - X_p) = \frac{4\pi}{\lambda_c} \cdot \frac{\gamma_t^2 \gamma_p^2 (X_t - X_p)^2 + Y_t^2 - Y_p^2}{2r_t(t_{st})} \quad (15)$$

A change in azimuth image position X_p is related to a quadratic phase expression for the SAR image. An estimator of the phase in azimuth direction will give an estimate of the target NRS.

3 Estimator for the normalised relative speed

The phase $\Phi(X_r X_p)$ will be equidistantly sampled in azimuth. In this paper, we use a one meter spacing between the sample points. These samples are used to build the vector $\Phi(n)$, where n is the sample index. From the chirp signal generated by the moving target, it is possible to estimate the target NRS. In [4], the finite difference operator Δ , which is defined as

$$\Delta\Phi(n) = \Phi(n) - \Phi(n-1) \quad (16)$$

is applied twice to the phase of a chirp, resulting in a quadratic component of the phase. If we denote the true chirp rate

$$\alpha = \Delta_x^2 \Phi(n) \quad (17)$$

the Gauss Markov estimator for α is defined as

$$\hat{\alpha} = \frac{1^T \mathbf{C}^{-1} \Delta_x^2 \Phi_m(n)}{1^T \mathbf{C}^{-1} 1} \quad (18)$$

where $\Phi_m(n)$ is the measurement vector of $\Phi(n)$ in the SAR image and \mathbf{C} is the covariance matrix of the noise in $\Delta_x^2 \Phi_m(n)$.

By solving Equation (15) for γ_t , the estimate of the NRS is obtained as

$$\hat{\gamma}_t = \left(\frac{1}{\gamma_p^2} - \frac{4\pi}{\lambda_c} \frac{1}{2r_t(t_{st}) \hat{\alpha}} \right)^{-\frac{1}{2}} \quad (19)$$

4 Results

The estimator $\hat{\gamma}_t$ is used in our experiments, both in simulation and on real data. In the first experiment, a SAR system with one receive antenna is simulated. The data which we use in our second experiment was collected by one of the antennas of the CARABAS-II system. The flight parameters for the real data, which also were the parameters used in simulations, are given in Table 1.

Height	3678m
Shortest distance to target	4572m
Transmission frequency	20-90MHz
Platform speed	129 m/s
Integration time	160 s

Table 1. SAR image formation parameters.

To meet the demand of good quality and ability to focus moving targets, the GBP algorithm is used.

The chirp estimate is found from Equation (18) by sampling the phase in the SAR image at the target minimum range. From the phase estimate, the NRS was found using Equation (19). In all SAR images in this paper, local range and local azimuth is used in which the

origin of the coordinate system is the first pixel of the local image. Between each image formation there is one estimation stage. In this paper, the estimation stages are numbered starting with stage 1 being based on the original image, stage 2 being based on the second image etc.

4.1 Simulation experiments

To illustrate the performance of the estimator given in Equation (19), simulations on an ideal point target were conducted. The target was moving at a speed of 5.4 m/s in the along-track direction. Using the simulation parameters in Table 1 and the target speed, NRS is found to be 0.9580. No noise was added in the simulation. First a SAR image is created, processed at ground speed. This original image can be seen in Figure 2a. Then, $\Phi_m(n)$ is extracted and the plot in Figure 2c was obtained.

After applying the estimator on the original image, the estimation yields an NRS of $\hat{\gamma}_t = 0.9550$, which correspond to an error in true relative speed of 0.4 m/s. Then, a second image is processed as illustrated in Figure 2b. The first estimate results in an overestimate of the NRS, i.e. the processed NRS is smaller than the target NRS. As expected from Equation (15), this will lead to a sign change in the quadratic term of the unwrapped phase $\Phi_m(n)$ as displayed in Figure 2d.

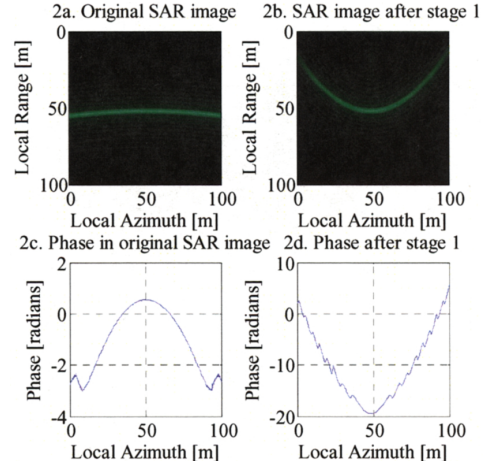


Figure 2. Simulation results of focusing of the target.

Applying the estimator twice, a good estimate is found, giving $\hat{\gamma}_t = 0.9583$ compared to the target NRS. In stage 2, the target energy is more focused, thus a better estimate is obtained. If we apply the estimator a third time, we get $\hat{\gamma}_t = 0.9580$ which allows for best possible focus of the target using the method in [6]. Processing for this estimate, we obtain Figure 3.

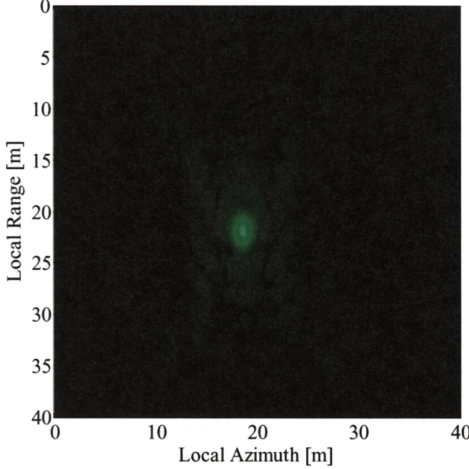


Figure 3. SAR image after focusing with the estimation after the third stage with an NRS of 0.9580.

4.2 Results on real data

The real data was collected by the CARABAS-II system and the parameters are given in Table 1. A moving target was detected in the SAR image and the target can be seen in Figure 4a. The target signature is found in the Baltic Sea, close to the coastline and is consequently some kind of a vessel. We assume this vessel to be a small ship. The quadratic phase in azimuth of the target is shown in Figure 4c. The phase is noisy and using real data, noise is an issue that will affect the quality of the estimation. The NRS estimate obtained from the original image is $\hat{\gamma}_t = 0.9704$. This estimate is used to process the image presented in Figure 4b.

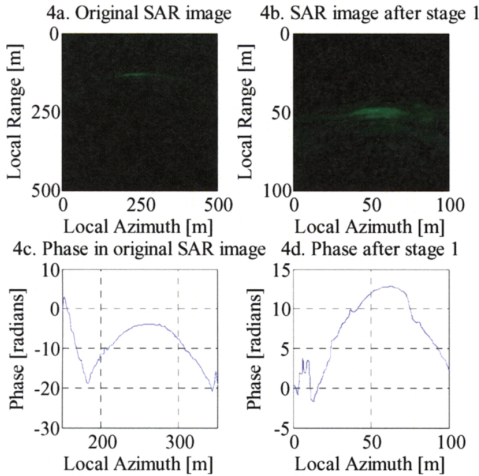


Figure 4. Results on real data of focusing of the target.

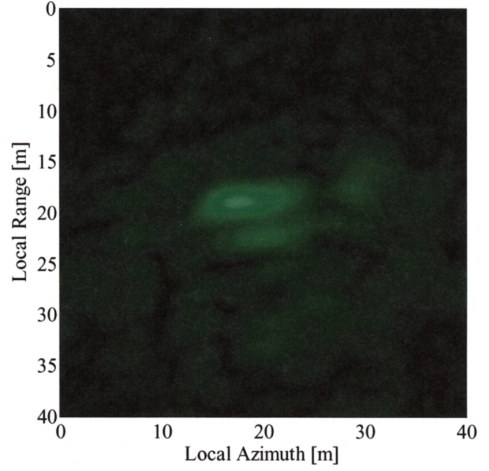


Figure 5. The SAR image after focusing with the second estimation of an NRS of 0.9596.

In this image, the target is more focused and the shape of the target has a much shorter extent. By focusing the energy along the azimuth direction, the Signal-to-Clutter Noise Ratio (SCNR) increases and the quality of the estimate will be improved. In stage 2, an estimate of $\hat{\gamma}_t = 0.9596$ is obtained. In [10], an estimate of the relative speed was found by the peak energy from the target. From that study the actual γ_t is found to be in the interval [0.9580, 0.9600]. Thus, we have a remarkably good result.

When considering Figure 4a as well as Figure 4b, one can see multiple ellipses. This indicates that the moving target either has multiple scatterers or the target accelerates during the integration time. This means that the target is not represented by a single NRS, since the ship will change speed constantly due to the waves in the water.

The image of the ship processed at $\gamma_p = 0.9596$ is shown in Figure 5. The 3dB width of the ship is approximately 8 meters in azimuth and 3 meters in range. This is a good result considering the target is a ship and not a point target.

5. Conclusions

We have derived an expression for the azimuth phase information, which allows estimation of NRS in SAR images. The method is based on a linear estimator and works in an iterative way. Both in simulation and on real data, the estimations from the method converge after a few iterations. Experiments on real data show that this method is a promising candidate for target NRS extraction. One advantage of this approach is that an estimate is obtained from a single antenna. Another advantage with this method is that it allows for estimating NRS even in the cases

where the energy of the target is weaker than surrounding targets.

Acknowledgements

The authors would like to thank the colleagues at the Swedish Defence Research Agency for the CARABAS-II SAR data supplied in this research. The authors would also like to thank the KK-Foundation for making this research project possible, and the support from Saab Bofors Dynamics, Saab Microwave Systems and Saab Space.

References

- [1] L.E. Andersson. "On Determination of a Function from Spherical Averages", *SIAM Journal of Applied Mathematics*, volume **19**, pp 214 - 341 (1988).
- [2] S. Axelsson. "Position Correction of Moving Targets in SAR-Imagery", In *Proceedings of SPIE - The International Society for Optical Engineering*, volume **5236**, pp. 80 - 92, (2004).
- [3] J.C. Curlander. "Synthetic Aperture Radar Systems and Signal Processing", John Wiley and Sons, New York, (1991).
- [4] P.M. Djuric and S.M. Kay. "Parameter Estimation of Chirp Signals", *IEEE Transactions on Acoustics, Speech and Signal Processing*, volume **38**, no. 12, pp. 2118 - 2126, (1990).
- [5] C.H. Gierull. "Ground Moving Target Parameter Estimation for Two-channel SAR", *IEE Proceedings on Radar, Sonar and Navigation*, volume **153**, no. 3, pp. 224 - 233, (2006).
- [6] H. Hellsten and L.M.H. Ulander. "Airborne Array Aperture UWB UHF Radar - Motivation and System Considerations", *IEEE Aerospace and Electronics Systems Magazine*, volume **15**, no. 5, pp. 35 - 45, (2000).
- [7] P.A.C. Marques and J.M.B. Dias. "Velocity Estimation of Fast Moving Targets Using a Single SAR Sensor", *IEEE Transactions on Aerospace and Electronic Systems*, volume **41**, no. 1, pp. 75 - 89, (2005).
- [8] M.I. Pettersson. "Detection of Moving Targets in Wideband SAR", *IEEE Transactions on Aerospace and Electronic Systems*, volume **40**, no. 3, pp. 780 - 796, (2004).
- [9] J.J. Sharma, C.H. Gierull and M.J. Collins. "The Influence of Target Acceleration on Velocity Estimation in Dual-channel SAR-GMTI", *IEEE Transactions on Geoscience and Remote Sensing*, volume **44**, no. 1, pp. 134 - 147, (2006).
- [10] V.T. Vu, T.K. Sjögren, M.I. Pettersson, H.-J. Zepernick and A. Gustavsson. "Experimental Results on Moving Targets Detection by Focusing in UWB Low Frequency SAR", In *Proceedings of IET International Radar Conference* (2007). In press.

II

Part II

A Comparative Study of the Polar Version with the Subimage Version of Fast Factorized Backprojection in UWB SAR

A Comparative Study of the Polar Version with the Subimage Version of Fast Factorized Backprojection in UWB SAR

T. K. Sjögren, V. T. Vu, M. I. Pettersson

Blekinge Institute of Technology

SE-371 79 Karlskrona, SWEDEN

email: thomas.sjogren@bth.se

Abstract: This paper presents a comparative study of the polar and the subimage based variants of the time domain SAR algorithm Fast Factorized Backprojection. The difference between the two variants with regard to the phase error, which causes defocusing in the image, is investigated. The difference between the algorithms in interpolation between stages is also discussed. To investigate the sidelobes in azimuth, the paper gives simulation results for a low frequency UWB SAR system for both algorithms. How the algorithms differ with regard to amount of beams and length of beams is also discussed.

1. Introduction

From the 1980s, interest for wide beam Ultra Wide Band (UWB) Synthetic Aperture Radar (SAR) increased due to its applications to high resolution and large area surveillance. The Fourier domain algorithms were unable to fully motion compensate the flight path in UWB SAR [1]. In response to this, time domain methods, which have the ability of UWB SAR imaging, were developed. The first time domain algorithm was Global Back Projection (GBP) [2]. The main advantages of GBP are the capability to produce high resolution SAR images and the much lower memory requirements for GBP compared to frequency domain algorithms, the disadvantage is that the algorithm consumes much more computation power compared to the traditional algorithms. From the 1990s, interest has grown within the area of SAR time domain processing and a couple of algorithms have been proposed which has the same benefit of motion compensation as GBP but at much lower computational cost [3-6]. First two stage algorithms [3-4] and later multi-stage algorithms [5-6] were developed giving further reduction in computation cost.

In [6], a multi stage time domain SAR algorithm called Fast Factorized Back Projection (FFBP) is introduced. One big advantage of FFBP compared to other multi-stage algorithms is that memory requirements can be traded against computation cost. FFBP is in [6] given in two variants, one polar and one subimage based variant. The two variants of FFBP have been introduced in the area of SAR [6-7], but to the knowledge of the authors only compared with each other within the area of Synthetic Aperture Sonar (SAS) [8-9].

2. Global Backprojection

GBP [2] is the backprojection of data from all pulses onto the Cartesian image grid. GBP is defined according to

$$h(x, \rho) = \int_{-\infty}^{\infty} g(x', R) R dx' , \quad (1)$$

where $R = \sqrt{(x'-x)^2 + \rho^2}$ is the range at aperture position x' , $g(x', R)$ is the radar echo, x and ρ are azimuth and range image coordinates respectively. When applying a frequency ramp filter, GBP exactly solves the SAR imaging inversion [2] for a straight flight track and can easily be extended for SAR imaging under any arbitrary geometry of radar data acquisition. Therefore it has been proven a powerful algorithm for SAR imaging. Evaluating the

backprojection integral for an aperture of size N and an image of size $N \times N$ corresponds to a computational cost proportional to N^3 . This is a much higher computational cost compared to the frequency domain algorithms, with a cost proportional to $N^2 \log N$, and also compared to the recent faster time domain SAR imaging algorithms with a cost down to $N^2 \log N$. Thus, when the SAR image is small, Global Backprojection [2] is a good choice due to the high SAR image quality obtained in combination with the low memory cost.

The strength in GBP's ability for high quality imaging for any data acquisition geometries is kept also with the faster variants of time domain imaging [3-6]. Algorithms [3-6] use the fact that the high Doppler frequency components of $g(x', R)$ changes slowly with x' , and therefore limits the sampling in Doppler direction, according to the Nyquist criterion as derived in [3].

3. Fast Factorized Backprojection

In this paper we study the two variants of the algorithm introduced in [6], namely a polar version and a subimage version of FFBP. We name the variants Polar-FFBP (PFFBP) and SubImage-FFBP (SIFFBP). In general FFBP starts with pulse compressed radar echoes, and then uses a variable amount of beam forming stages before the final stage where the beams are backprojected onto the Cartesian image grid. The main differences of the two versions of FFBP are that the PFFBP samples the beams equidistantly in cosine of angle and that PFFBP does not apply factorization of the beams in range direction as illustrated in Figure 1. With regard to computational cost, both algorithms perform equal. The core of FFBP is the generation of new beams, based on old beams. This process is described according to [6] as the discrete version of

$$h(x, \rho) = \sum_{i=-\infty}^{+\infty} h(x_i, r_i, \vartheta_i) = \sum_{i=-\infty}^{+\infty} \sum_{j=-\frac{n-1}{2}}^{+\frac{n-1}{2}} h_{\frac{j}{n}} \left(x_0 + (ni + j) \frac{d}{n}, r'_j, \vartheta'_j \right) = \sum_{l=-\infty}^{+\infty} h_{\frac{l}{n}} \left(x_0 + l \frac{d}{n}, r'_l, \vartheta'_l \right) \quad (2)$$

$$r'_j = \sqrt{(r_i \cos \vartheta_i + x_i + x'_j)^2 + (r_i \sin \vartheta_i)^2}, \quad \vartheta'_j = \arctan[r_i \sin \vartheta_i / (r_i \cos \vartheta_i + x_i - x'_j)]$$

Where r_i and ϑ_i is range and angle in the polar coordinate system with origin at the subaperture centre, and i index of subaperture and j index of sub-subaperture.

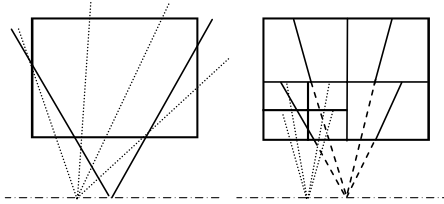


Figure 1. Beams in two stages of PFFBP and SIFFBP. Beams in stage 2 are dotted.

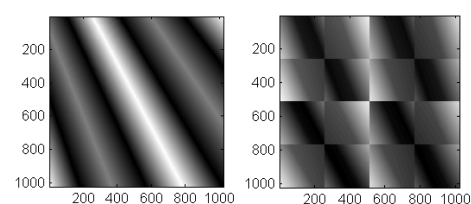


Figure 2. Phase error distribution in image through two stages of PFFBP and SIFFBP.

As seen in Figure 1, the amount of beams in SIFFBP is much higher, as the beam sampling density in angle increases with slantrange position of the subimage. However, the beam length is much shorter than for PFFBP which saves memory. It should also be noted that using nearest neighbour interpolation in angle, more than one parent beam always has to be considered. However, SIFFBP overcomes the need for multiple beams by not strictly using nearest neighbour, instead the parent beam for the parent subimage is used directly. Thus, the interpolation between stages for SIFFBP is already inherent in the algorithm and is therefore very fast.

One other aspect of SIFFBP is its possibility of arbitrarily factorizing the subimages. This allows for subimages of different size over the image area, as well as a change in size of subimages with regard to the position of the subaperture. The earlier corresponds to areas further away on the image having larger subimages, thus reducing the computational cost of the SAR processing. The latter due to the fact that near range change for different subapertures. Another aspect of differences between the two variants is that in SIFFBP, the sampling in the Fourier domain is not equidistant in angle with more samples at high angles, while it is evenly distributed in angle for the polar version.

4. Error analysis

In [6] an error analysis is performed, where the maximum phase error due to nearest neighbour interpolation in angle at each stage of the algorithm is derived. According to [6], the maximum phase error for each stage is given by $2k\Delta R$, where ΔR is the range error

$$\Delta R = \sqrt{r^2 + t^2 - 2rt \cos(\vartheta + \phi)} - \sqrt{r^2 + t^2 - 2rt \cos \vartheta} . \quad (3)$$

where r is range to the image pixel from the subaperture centre, t is distance from subaperture centre to the aperture position considered, ϑ is the angle to the image pixel position and ϕ the angle between the pixel and the beam centre. In [6] an upper bound for the absolute value of the range error is derived according to

$$|\Delta R| \leq \frac{dD}{4r}, \quad (4)$$

where d is subaperture size and D is subimage size.

In Figure 2, the range error is shown for the two algorithms. The total range error is given in the SAR image using nearest neighbour interpolation. The images in Figure 2 were generated considering the error according to (3) for one subaperture through the two first stages of the algorithm. In the first stage 2 beams were used and in the second stage 4 beams corresponding to 4 subimages in first stage and 16 in the second. In the images the bright areas correspond to high range error, thus giving more defocusing in these areas. One observation is that the error for PFFBP is high in the centre of the image which is connected to the location in the middle of two beams in both stages. For SIFFBP, the error is higher in the corners of each subimage.

5. Simulation results

To evaluate the two variants, simulations of a point targets have been made using parameters according to the CARABAS-II system. The aperture size is 4096 positions and the aperture step size is 0.83 m. Near range of the image is 1414 m and the image size is 1024x1024 pixels. The images where formed using 4 stages, with a factorization step of 4 in each stage, corresponding to a maximum range error of 0.18m or $\lambda_{min}/17$ in each stage according to (4). For interpolation in range, upsampling was used. In angle, nearest neighbour was used. In the simulation, the settings are selected so that both algorithms have the same maximum range error throughout stages and the same computational cost.

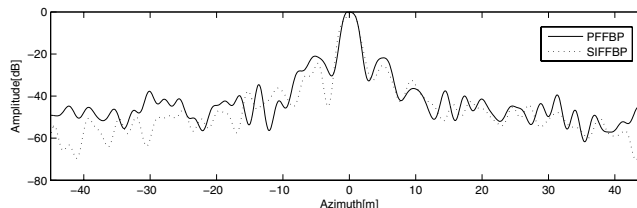


Figure 3. Azimuth sidelobes around simulated point target.

The ISLR obtained for SIFFBP is -13.6dB, while for PFFBP -14.7dB is obtained. As seen in Figure 3, the algorithms give similar peak levels of sidelobes, being able to suppress the sidelobes to approximately -20dB.

5. Conclusions and discussion

The paper has shown that in SAR imaging the two algorithms perform at a similar level with regard to image quality and that the obtained sidelobe level and ISLR can be good even without the use of angular interpolation kernels. The paper has also highlighted the differences of the two algorithms and shown the error distribution over the image scene. Another important issue is the possibility of extending the algorithms for use with microwave SAR. In microwave SAR, autofocusing is often necessary for being able to correct the movements of the platform. When autofocusing, it is advantageous to have a strong scatterer in the scene. In the polar version of FFBP, the beams cover a larger extent of the image and therefore it is more likely there is at least one strong scatterer in the beam, allowing for more successful autofocus for each beam.

References:

- [1] Ulander L.M.H., Fröling P.-O., "Precision processing of CARABAS HF/VHF-band SAR data", *Proceedings of IGARSS 1999*, Hamburg, Germany, 28.6-2.7.1999, vol 1, pp47-49.
- [2] Andersson L.E., "On Determination of a Function from Spherical Averages", *SIAM Journal of Applied Mathematics*, 1988, vol 19, pp214-341.
- [3] Yegulalp A.F., "Fast backprojection algorithm for synthetic aperture radar", *IEEE Radar Conference 1999*, Waltham, USA, 20-22.4.1999, pp60-65.
- [4] Seger O., Herberthson M., Hellsten H., "Real-time SAR processing of low frequency ultra wide band radar data", *Proceedings of EUSAR'1998*, 25-27.5.1998, Friedrichshafen, Germany, pp489-492.
- [5] McCorkle J.W., Rofheart M., "An order $N^2 \log(N)$ backprojector algorithm for focusing wide-angle wide-bandwidth arbitrary-motion synthetic aperture radar", *Proceedings of SPIE*, 1996, vol 2747, pp25-36.
- [6] Ulander L.M.H., Hellsten H., Stenström G., "Synthetic-aperture radar processing using fast factorized back-projection", *IEEE Transactions on Aerospace and Electronic Systems*, 2003, vol 39, pp760-776.
- [7] Fröling P.-O., Ulander L.M.H., "Evaluation of angular interpolation kernels in fast back-projection SAR processing", *IEE Proceedings in Radar, Sonar and Navigation*, 2006, vol 153, pp243-249.
- [8] Callow H.J., Hansen R.E., Saebo T.O., "Effect of Approximations in Fast Factorized Backprojection in Synthetic Aperture Imaging of Spot Regions", *Oceans 2006*, Boston, USA, 18-21.9.2006, pp1-6.
- [9] Shippey G., Banks S., Pihl J., "SAS Image reconstruction using Fast Polar Back Projection: comparisons with Fast Factored Back Projection and Fourier-domain imaging", *Oceans 2005 Europe*, Brest, France, 20-23.06.2005, vol 1, pp96-101.

Part III

Moving target relative speed
estimation in the presence of
strong stationary surrounding
using a single antenna UWB
SAR system

III

MOVING TARGET RELATIVE SPEED ESTIMATION IN THE PRESENCE OF STRONG STATIONARY SURROUNDING USING A SINGLE ANTENNA UWB SAR SYSTEM

T.K. Sjögren, V.T. Vu, M.I. Pettersson

Blekinge Institute of Technology (BTH), Department of Signal Processing
P.O. Box 520, SE-372 25 Ronneby, Sweden

E-mail: thomas.sjogren@bth.se, Fax: +46 457 27914, Phone: +46 733 38 47 88

ABSTRACT

This paper investigates how relative speed estimation of moving targets in Synthetic Aperture Radar (SAR) images is affected by strong stationary surrounding clutter. The result extends previous work by estimating moving target relative speed under the influence of clutter and Gaussian noise. The results obtained show that good estimates can be obtained even in situations with relatively high clutter and noise, i.e. SNR and SCR lower than 10dB.

Index Terms— Synthetic Aperture Radar, Speed Estimation, Ultra Wide Band, Moving Targets

1. INTRODUCTION

In the area of remote sensing it is of great interest to image the earth from air- or space based sensors. In response to this, a wide variety of sensors have been developed and used on space- and airborne missions. One of these is radar, which has the unique capability to form remote sensing images independent of weather conditions and daylight. The fact that the radiating source is extremely well known in space and time is a strong advantage of radar compared to optical and other passive sensors. The known source gives radar unique capabilities to detect changes and motion, such as glacier drift to moving target detection. Also, Synthetic Aperture Radar (SAR) is a very strong remote sensing instrument due to its ability to form images with very high resolution at any range.

There are some problems when imaging with SAR, one is to handle the motion compensation needed for Ultra Wide Band (UWB) systems. This problem grows with increasing integration angle and for airborne systems this is normally more critical than for spaceborne systems. To minimize the errors in motion compensation for UWB SAR and to obtain a focused image, time domain backprojection algorithms are

best suited [1]. In this research Global Backprojection [2] (GBP) is applied, which is the time domain algorithm that has highest computational cost but also highest accuracy. However, the results of this work are valid with other algorithms. Another effect associated with SAR is that when a moving target is present, the target will be displaced and smeared. Depending on integration time and the relative speed between target and platform, the smearing effect of the target will be more or less severe. However, this effect can be used to detect and to estimate the target properties. To focus a moving target many different approaches have been suggested. If the target is moving with constant speed during the integration time, the target can be focused if a new SAR image is processed using the targets normalized relative speed (NRS) [3]. In [4] an iterative procedure for focusing moving targets based on NRS estimates was presented and tested on data from the CARABAS-II system having a moving target at sea. Even though this system is a low frequency UWB SAR system having long integration time, results were promising, with good focus obtained after two iterations.

This paper presents a study how NRS estimation accuracy is affected by the presence of strong stationary surrounding scatterers. The study consists in simulations of a SAR system according to the specifications of the CARABAS-II SAR, relating to the good experimental results found in [4-5]. However in [4-5] the target was found in an area with low clutter backscatter. This work therefore also relates to the existing low frequency systems at UHF. The lower frequency (VHF, UHF) bands are chosen, due to their strong ability to penetrate vegetation. The reason why the influence of stationary targets is concerned in this paper is that when using the long wavelengths and UWB systems, the background is low and most stationary objects act as very strong point targets. The effect of added white Gaussian noise in the SAR image is also investigated. The effect of the noise should illustrate the behavior of the estimator in microwave SAR where the clutter behaves similar to noise.

¹ The Authors would like to thank the KK-Foundation for making this research possible, and the support from Swedish Defence Research Agency, Saab Bofors Dynamics, Saab Microwave Systems and Saab Space.

2. SPEED ESTIMATION FOR MOVING TARGETS IN SYNTHETIC APERTURE RADAR

When estimating speed for moving targets, different approaches can be undertaken. These approaches can mainly be divided into two groups, phase based or amplitude based. The phase based approaches estimate the phase of the moving target in the raw data or in the SAR image. Normally, the phase chirp rate in azimuth is used for estimating the speed of the target [6-10]. The amplitude based approaches also consider the phase, however they focus the target for a set of speeds [5,11]. These algorithms are both used in the detection and the estimation phase. The speed which gives best focus is the most likely speed. The phase based approach has the advantage that for obtaining an estimate of the moving target speed, no SAR processing is needed and by that has a lower computational cost. The latter approach has the advantage that it focuses all energy and therefore increases the signal to clutter ratio. A third approach for estimating the motion parameters of a moving target is to create a set of SAR images and for each image estimate the image coordinates of the moving target. The set of estimated positions is used for estimating the speed of the moving target [12].

For estimating the chirp rate in a SAR image, which is needed for the phase based approaches; one can apply mainly two different methods. The first method is based on transforming the complex signal containing the moving target into a time-frequency domain by use of e.g. Wigner-Ville transform or the ambiguity function. Then, the Hough transform is used in order to obtain the estimate of the speed. The other method is to apply a phase unwrap on the signal containing the moving target and then apply the finite difference operator twice. After this apply for instance the Gauss Markov estimator as proposed in [4]. This last method is used in this paper and its core can be described by Equation 1 and Equation 2 [4].

$$\hat{\alpha} = \frac{\mathbf{1}^T \mathbf{C}^{-1} \Delta_x^2 \Phi_m(n)}{\mathbf{1}^T \mathbf{C}^{-1} \mathbf{1}} \quad (1)$$

$$\hat{\gamma}_t = \left(\frac{1}{\gamma_p^2} - \frac{4\pi}{\lambda_c} \frac{1}{2r_t(t_{st})} \frac{1}{\hat{\alpha}} \right)^{-\frac{1}{2}} \quad (2)$$

Where α is the chirp rate in azimuth of the moving target in the SAR image, γ_p is the NRS used when SAR processing and γ_t is the NRS of the moving target. \mathbf{C} is the covariance matrix of the clutter and noise and $\Delta_x^2 \Phi_m(n)$ is the second derivative of the measured phase, where the phase is measured as explained in [4]. The centre wavelength is λ_c and $r_t(t_{st})$ is the true range to the target at time of stationary phase.

3. MOVING TARGET FOCUSING USING NRS

As the SAR sensor moves along a synthetic aperture, the range to any coordinate on ground is given by

$$r(\xi, \eta, t) = \sqrt{(v_{pl}t - \xi(t))^2 + \eta(t)^2 + h^2} \quad (3)$$

Where ξ and η are the ground coordinates in the along-track direction and the cross-track direction, respectively, h is the flight altitude of the sensor, t is time and v_{pl} is the speed of the SAR platform. Assuming no target accelerations and let X_t and Y_t denote the coordinates of a focused target having NRS γ_t . The range to the target from the platform can be described by

$$r_t(t) = \sqrt{\gamma_t^2 (v_{pl}t - X_t)^2 + Y_t^2} \quad (4)$$

Where the NRS γ_t , which depends on target speed in along-track v_ξ and cross-track v_η , is defined by

$$\gamma_t = \sqrt{\frac{(v_{pl} - v_\xi)^2 + v_\eta^2}{v_{pl}^2}} \quad (5)$$

We now let X_p and Y_p denote image coordinates for a SAR image processed at the NRS γ_p . The range from the sensor to an arbitrary image coordinate will then be given by

$$r_p(X_p, Y_p, t) = \sqrt{\gamma_p^2 (v_{pl}t - X_p)^2 + Y_p^2} \quad (6)$$

We now see that if γ_t of the target is known, we can focus the target at $(X_p, Y_p) = (X_t, Y_t)$ in the SAR image, if we choose $\gamma_p = \gamma_t$.

4. SIMULATION EXPERIMENT SETUP

Two simulation experiments were undertaken, illustrated in Figure 1 and Figure 2. In both experiments, the moving target under interest was distorted by clutter or noise in which the clutter was modeled as a point scatterer and the noise as additive white Gaussian noise. Our signal model for the SAR image in azimuth direction around the target is given in Equation 7.

$$z(X) = A_s e^{j2\pi(\phi_{0,s} + \frac{\alpha_s}{2} X^2)} + A_c e^{j2\pi(\phi_{0,c} + \frac{\alpha_c}{2} X^2)} + w \quad (7)$$

Where X is azimuth image coordinate and w is the additive Gaussian noise sequence having variance σ_n^2 . The amplitude and initial phase of the moving target and stationary scatterer is given by A_s , A_c , $\phi_{0,s}$ and $\phi_{0,c}$. The azimuth chirp rate which we want to estimate using Equation 1 is α_s , while α_c is the chirp rate of the stationary target.

Note that A_s and A_c will be different for each processing NRS due to the focusing effect [5]. However, for evaluation purposes, we can find these values for each processing speed we want to evaluate.

We define the Signal-to-Noise Ratio (SNR) and Signal-to-Clutter Ratio (SCR) according to Equation 8 and Equation 9. From these definitions one easily finds Clutter-to-Noise Ratio (CNR).

$$SNR = \frac{A_s^2}{\sigma_n^2} \quad (8)$$

$$SCR = \frac{RCS_s}{RCS_c} \quad (9)$$

To find the σ_n^2 which correspond to a certain SNR and A_s , we form the SAR image of only the moving target at the given NRS and choose the peak in the image as the signal amplitude. SCR is simply defined as the ratio between the radar cross sections (RCS) of the moving target and the stationary scatterer.

In SAR image formation, we use Global Backprojection (GBP) with an upsampling factor of 20 and a linear interpolation kernel. Simulation parameters used for both experiments are given in Table 1. They are the same system parameters as used in [4].

In the first experiment the moving target is distorted mainly by the point scatterer which is positioned in the track of the moving target. This is a simple way to model the kind of clutter which characterizes UWB VHF SAR, which means large scatterers that are often well separated and each acts similar to point scatterers. With the system parameters in Table 1, there will be only one point scatterer in the resolution cell that causes this special clutter selection. In this experiment we extend the approach proposed in [4] by estimating the covariance of the stationary scatterer and compare with results achieved without taking the covariance of the stationary scatterer into account.

In the second experiment, the moving target is mainly distorted by the white Gaussian noise. This is to characterize the kind of distortion from clutter which occurs in microwave SAR. The noise is generated as white Gaussian noise in Matlab and for each SNR, 1000 noise distorted images are generated and the estimator is applied for each. From this set of estimates, the variance and the mean is calculated and this is displayed in Figure 3 and Figure 4.

Shortest distance to target	4275m
Transmission frequency	20-90MHz
Platform speed	129 m/s
Integration time	160 s
Target speed	5.4 m/s, i.e. NRS of 0.958
Processing NRS	0.93

Table 1. SAR image formation parameters.

5. SIMULATION RESULTS

The results obtained for the two simulation experiments are displayed in Figure 3 and Figure 4. In Figure 3 by extending the approach suggested in [4] considering the covariance matrix of the stationary scatterer, we obtain very

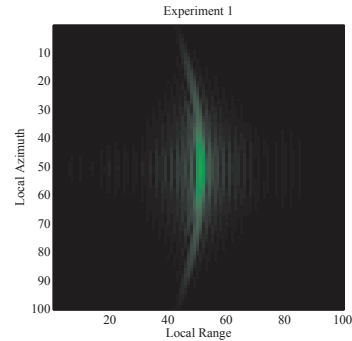


Figure 1. Moving target with defocused stationary target (SCR=3dB).

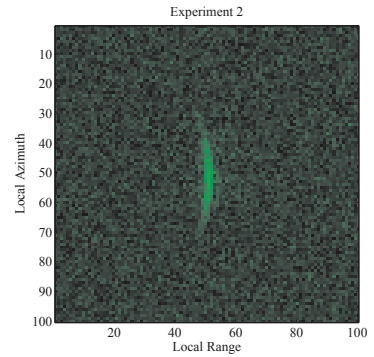


Figure 2. Moving target in Gaussian noise (SNR=3dB).

close to the same results as covariance matrix based on an independent noise background as in [4]. For SCR of approximately 5 dB and above, error in the mean of the estimate is very low, even below 0.01 in NRS. This corresponds to an error of 1m/s in relative speed. This means that the estimate in the next iteration converge towards the true NRS. One could argue these errors are quite high. However, the estimates in this study are not final estimates, only first iteration estimates and as in [4] there should be further estimates to get the correct speed. Further iterations are not considered here because the purpose of this study is to investigate the effect of strong stationary surrounding upon the first iteration estimates.

In Figure 4 we see that the variance decreases until approximately 7dB, after which it is very small. However, already at such low SNR as 4dB, we can see that the mean estimate is good and the variance is about 0.01 NRS, thus allowing for good first iteration estimates. This is a promising result, as it means that if we just detect a target with very low signal level compared to a noisy background, we can be able to get a good first iteration estimate and will be able to converge into a good final NRS estimate.

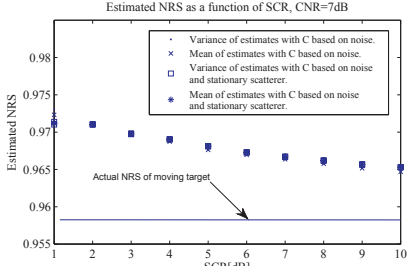


Figure 3. Estimated NRS as a function of SCR. The CNR was chosen to 7dB.

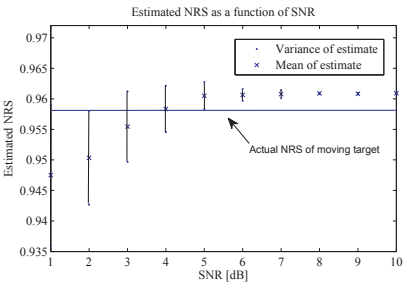


Figure 4. Estimated NRS as a function of SNR. All outliers having estimates over 2 were excluded. This was because the variance of the estimate varied strongly between runs due to outliers. At most 5 estimates in 1000 were excluded.

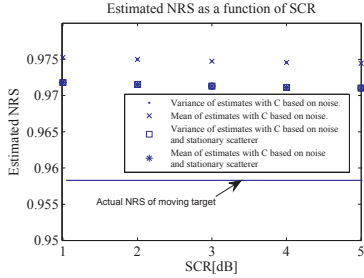


Figure 5. Estimated NRS as a function of SCR, $\gamma_p = 1$.

A further simulation experiment was made, where the Processing NRS was changed to 1, i.e focusing for a stationary scene. The result is shown in Figure 5. When taking the covariance of the stationary target into account, the first estimate is better compared to when the covariance matrix is only based on noise.

It should further be noted that the estimator has a bias even at high SCR or SNR. It has been found in the simulation experiments that when varying target NRS from a value near processed NRS to values further away from processed NRS, this bias will increase.

6. CONCLUSIONS AND DISCUSSION

The work presented in this paper shows that good estimates of moving target relative speed can be obtained by a UWB SAR system. The results can be obtained even when SCR or SNR is relatively low. The threshold is around 4dB for SNR and about 5dB for SCR in order to obtain good first iteration estimates. The main contributions of this work is to investigate the behavior of the estimator introduced in [4] and finding estimation thresholds with regard to SCR and SNR as well as extending the approach by estimating the covariance matrix of the clutter. The results show the thresholds are low in both SNR and SCR. A final conclusion is that when taking the clutter into account when estimating the covariance matrix an improvement is obtained when SAR processing for a stationary scene.

6. REFERENCES

- [1] L.M.H. Ulander, P.-O. Frörlind, "Precision processing of CARABAS HF/VHF-band SAR data," *Proceedings of IGARSS 1999*, Hamburg, Germany, pp. 47-49, 1999.
- [2] L.E. Andersson, "On determination of a function from spherical averages," *SIAM Journal of Applied Mathematics*, pp. 214-341, 1988.
- [3] H. Hellsten, L.M.H. Ulander, "Airborne array aperture UWB UHF radar – motivation and system considerations," *IEEE Aerospace and Electronic Systems Magazine*, pp. 35-45, 2000.
- [4] T.K. Sjögren, V.T. Vu, M.I. Pettersson, H.-J. Zepernick, and A. Gustavsson, "Speed estimation experiments for ground moving targets in UWB SAR," *Proceedings of IET International Radar Conference*, Edinburgh, UK, 2007.
- [5] V.T. Vu, T.K. Sjögren, M.I. Pettersson, H.-J. Zepernick and A. Gustavsson, "Experimental results on moving targets detection by focusing in UWB low frequency SAR," *Proceedings of IET International Radar Conference*, Edinburgh, UK, 2007.
- [6] F. Zhou, R. Wu, M. Xing, and Z. Bao, "Approach for single channel SAR ground moving target imaging and parameter estimation," *IET proceedings in Radar, Sonar and Navigation*, pp. 59-66, 2007.
- [7] S. Barbarossa, A. Farina, "Detection and imaging of moving targets with synthetic aperture radar. 2. Joint time-frequency analysis by Wigner-Ville distribution," *IEE Proceedings in Radar and signal processing*, pp 89-97, 1992.
- [8] S. Barbarossa, "Analysis of multicomponent LFM signals by a combined Wigner-Hough transform," *IEEE Transactions on Signal Processing*, pp 1511-1515, 1995.
- [9] M. Wang, A.K. Chan, C.K. Chui, "Linear frequency-modulated signal detection using Radon-ambiguity transform," *IEEE Transactions on Signal Processing*, pp. 571-586, 1998.
- [10] J.C. Wood, D.T. Barry, "Radon-transformation of time-frequency distributions for analysis of multicomponent signals," *IEEE Transactions on Signal Processing*, pp. 3166-3177, 1994.
- [11] C. H. Gierull, "Ground moving target parameter estimation for two-channel SAR", *IEE Proceedings on Radar, Sonar and Navigation*, pp 224-233, 2006.
- [12] M. Kirsch, "Detection and imaging of arbitrarily moving targets with single-channel SAR", *IEE Proceedings on Radar, Sonar and Navigation*, pp 7-11, 2003.

Part IV

Moving Target Relative Speed Estimation and Refocusing in Synthetic Aperture Radar Images

IV

Moving Target Relative Speed Estimation and Refocusing in Synthetic Aperture Radar Images

Thomas K. Sjögren, *Student Member, IEEE*, Viet T. Vu, *Student Member, IEEE*,
Mats I. Pettersson, *Member, IEEE*, Anders Gustavsson, and Lars M. H. Ulander, *Senior Member, IEEE*

Abstract—In this paper, a method for moving target relative speed estimation and refocusing based on Synthetic Aperture Radar (SAR) images is derived and tested. The estimation is based on a chirp estimator that operates in the SAR image and the refocusing of the moving target is made locally using subimages. Focusing of the moving target is achieved in the frequency domain by phase compensation. Focusing in this way makes it even possible to handle large range cell migration. The proposed approach is tested in a simulation and using real Ultra Wide Band (UWB) SAR data with satisfying results. The estimation method works especially well in connection with UWB SAR, where the clutter is well focused and the phase of the spread out moving target signal becomes less distorted. The main limitation of the approach is target accelerations where the distortion increases with the integration time.

Index Terms—SAR, radar, remote sensing, moving targets, speed estimation, SAR processing.

I. INTRODUCTION

When observing the Earth from spaceborne or airborne platforms with the use of imaging sensors such as Synthetic Aperture Radar (SAR) or optical sensors, it is possible to observe climate change, classify forest

T. K. Sjögren, V. T. Vu and M. I. Pettersson are with Blekinge Institute of Technology (BTH), Ronneby, 37225 Sweden. E-mail: thomas.sjogren@bth.se. A. Gustavsson and L.M.H. Ulander are with the Swedish Defence Research Agency (FOI)

Manuscript received February 13, 2010.

and crop types and monitor effects of earthquakes. In the case of an optical sensor, the image is obtained during an extremely short time which is decided by the shutter opening time. In the case of a SAR system, however, the data is gathered over several seconds and even minutes. Further comparing the two types of sensors, SAR is able to operate in bad weather and during the night. SAR is also capable of detecting change and movement. It is possible to detect e.g. moving ships or other vehicles on the ground. Such information can be used for many different applications e.g. surveillance of ships and traffic [1], [2]. In order to obtain good results for the purpose of e.g. traffic monitoring, the SAR system should be equipped with at least two antennas physically separated in the flight direction.

In Narrow Band (NB) SAR, which also can be referred to as conventional SAR, the bandwidth of the signal is normally small compared to the center frequency, often less than 10 percent. Two examples of conventional SAR systems are the space borne Radarsat-2 [3] and TerraSAR-X [4]. Such systems often have integration angles of less than 10 degrees. These conditions require SAR processing algorithms such as Chirp Scaling (CS) [5] to form the images. NB SAR systems often operate at high center frequencies. This allows for a high resolution in the SAR image in terms of both range

and azimuth, even when only a low integration angle and a low relative bandwidth are available. However, the higher the resolution, the better the ability to detect and separate targets. If very high resolution is of interest, larger relative bandwidths and larger integration angles are needed. In these cases, Ultra Wide signal bandwidth and Ultra Wide beamwidth is needed. We denote such systems UWB-SAR systems.

If there is an interest in imaging the ground in forested areas, the Foliage Penetrating (FOPEN) capability characteristic of Low Frequency (LF) SAR can be utilized. LF SAR systems must at the same time make use of UWB SAR in order to obtain good resolution. LF SAR in combination with UWB is related to extreme conditions such as very long integration times as well as a truly hyperbolic target range history. These conditions demand that either algorithms such as Range Migration [6] or any of the family of Back Projection algorithms, e.g. Global Backprojection (GBP) [7], are used if good image quality is to be obtained. When combining foliage penetration with the previously mentioned SAR abilities, it is possible to detect changes under foliage [8].

Usually in SAR images, the signature of a moving object is contained in one range cell. In this case, a one dimensional matched filter can be applied locally in order to focus the moving target. However, the signature of moving objects in UWB-SAR images spreads over multiple range cells. In these cases, a one dimensional matched filter will be insufficient. Therefore, the refocusing method needed to obtain a high resolution image of the moving target based on a SAR image depends strongly on the system parameters.

Many earlier methods have been presented that estimate the speed of moving targets in SAR imagery [9]- [14]. In [15], a method for estimating Normalized Relative Speed (NRS) is presented using subapertures.

There are also methods which estimate target acceleration, as presented, e.g., in [10]. When using single channel SAR, only one degree of freedom is usually available for parameter estimation. Because of this, only the speed parameter in the along-track or the across-track direction can be measured, while the use of more antennas allows for more degrees of freedom. Some recent publications show solutions to how to estimate more than one parameter using single channel SAR data. Once the parameters have been estimated, it is also important to obtain a focused SAR image. Different methods have been suggested for this process. For instance, based on an estimate of the speed parameter, GBP can be used to form a focused, very small SAR image that surrounds the moving target [16]. Other methods apply a matched filter to the final SAR image or use an interpolation in the 2D frequency domain such as in [17], allowing for high-quality refocusing of SAR images with long integration times, such as those produced by UWB SAR systems. In the refocusing methods given in [17], the basic assumption is that the original SAR image was produced to image stationary objects on the ground.

In this paper, a method to estimate the speed and refocus an object moving on the ground is presented. The method is based on estimating the speed by using the phase information in a SAR image. The model used to acquire the phase information used in this paper is a more general version compared to the one developed in [16]. Also, a method to refocus a moving target in a SAR image is presented. In this paper, the refocusing equation is derived for a general case when the original SAR image was formed with an arbitrary focusing speed, making it more general compared to [17].

This paper is divided into eight sections. In section II, the radar model used and the theory of SAR moving target focusing employing normalized relative speed (NRS)

is presented. In section III, an analytical expression for the phase of a moving target in a SAR image is presented. The procedure for obtaining the NRS estimate is presented in section IV and in section V the refocusing method of the SAR image is derived. Section VI shows results based on simulations and in Section VII, results from using a real SAR image with a simulated target superimposed is presented. Finally, in section VIII the results of the paper are discussed and conclusions drawn.

II. THE RADAR MODEL AND MOVING TARGET FOCUSING

To estimate speed and to refocus the SAR image, a model is needed. The model used in this paper is based on a set of assumptions. We assume a point target, that the signal sent from the SAR system is a chirp signal, a straight flying platform above a flat earth and that the start-stop approximation is valid. Thus, a signal model where the received signal is a time-shifted and attenuated version of the transmitted signal is attained. If we are dealing with a chirp signal, and if the pulse compressed signal is much shorter than the pulse length, the pulse compressed signal before SAR processing for a target that has the range history $R_t(t)$, where t is slow time, is given by (1):

$$s_{pc}(\tau, t) = \frac{T_p}{R_t(t)^2} e^{j2\pi\left(\frac{2R_t(t)}{c}-\tau\right)f_c} \text{sinc}\left(2\pi k T_p \left(\frac{2R_t(t)}{c}-\tau\right)\right) \quad (1)$$

where τ is fast time, T_p is the pulse length, k is the chirp rate and f_c is the center frequency of the radar signal.

If a target is moving on the ground from the position $(x_1, y_1, 0)$ to $(x_2, y_2, 0)$ during the SAR illumination time with no acceleration and at a constant speed, we can parametrize the position.

$$\begin{aligned} x_{tc}(t) &= v_x(t - t_0) + x_0 \\ y_{tc}(t) &= v_y(t - t_0) + y_0 \\ z_{tc}(t) &= 0 \end{aligned} \quad (2)$$

where t_0 is the time where the distance is at the minimum between the target and the platform and x_0 is the position of the target at t_0 .

In the same coordinate system we can also write the movements of the SAR platform with constant speed v_{pl} , moving parallel with the x-axis. The platform movements can be written as

$$\begin{aligned} x_{pc}(t) &= v_{pl}t \\ y_{pc}(t) &= 0 \\ z_{pc}(t) &= h \end{aligned} \quad (3)$$

and the range between the target and the platform in cartesian coordinates can be described according to

$$R(v_x, v_y, v_{pl}, t) = \sqrt{(v_{pl}t - v_x(t - t_0) - x_0)^2 + (v_y(t - t_0) - y_0)^2 + h^2} \quad (4)$$

Now, if we want to make a SAR image in which we focus a target with the parameters x_0, y_0, v_x, v_y , we can rewrite (4) using image coordinates. These are cylindrical coordinates, and they take on the following form:

$$R_t(t) = \sqrt{\gamma_t^2 (v_{pl}t - X_t)^2 + Y_t^2} \quad (5)$$

Identifying the t^2 coefficients in (4) and (5), we get the NRS as well as expressions for the image coordinates X_t and Y_t according to [18]

$$\gamma_t = \sqrt{\frac{(v_{pl} - v_x)^2 + v_y^2}{v_{pl}^2}} \quad (6)$$

and

$$X_t = x_0 - \frac{v_y}{(v_{pl} - v_x)} y_0 \quad (7)$$

$$Y_t = \sqrt{h^2 + y_0^2 \left(1 + \frac{v_y^2}{(v_{pl} - v_x)^2} \right)} \quad (8)$$

where $t_0 = \frac{X_t}{v_{pl}}$ from (5) was used [18]. Based on this expression for a moving target range history, we are able to process the SAR scene using

$$R_p(t) = \sqrt{\gamma_p^2 (v_{pl}t - X_p)^2 + Y_p^2} \quad (9)$$

where γ_p is the processing NRS, X_p is the azimuth image coordinate and Y_p the slanrange image coordinate in order to focus all targets with $\gamma_t = \gamma_p$.

III. PHASE OF A MOVING TARGET IN A SAR IMAGE

Starting with the expression for the pulse compressed chirp signal given in (1), we know that we can focus a moving target if $\gamma_p = \gamma_t$. At the same time as we focus a moving target, all scatterers with other NRSs will become defocused.

In SAR processing, phase is fundamental. When looking at a defocused target, information about its phase will be essential in order to be able to estimate the speed of the target. Therefore, finding the phase from a target with γ_t in a SAR image processed at γ_p is important.

Using the Global Back Projection integral [7], we can write the image response as

$$h(X_p, Y_p) = \int_{-\infty}^{\infty} s_{pc}(\tau, t) R_t(t) dt \quad (10)$$

where X_p and Y_p are the processed SAR images pixels and s_{pc} is the pulse compressed target radar echo.

If we again consider (1) and make the change of variable $\tau = \frac{2R_p(t)}{c}$, we can rewrite (1) into (11)

$$\begin{aligned} s_{pc}(\tau, t) &= \frac{T_p}{R_t(t)^2} e^{i\frac{4\pi f_c}{c}(R_t(t) - R_p(t))} \\ &\cdot \text{sinc}\left(\frac{4\pi k T_p}{c}(R_t(t) - R_p(t))\right) \end{aligned} \quad (11)$$

Inserting (11) into (10), the integral in (10) can now be approximated using stationary phase approximation. In other words, we assume that at the point (X_p, Y_p) in the final SAR image, the phase from the moving target is the phase corresponding to when $|R_t - R_p|$ is at the minimum.

In order to find the time of the stationary phase t_{st} , we take the derivative with respect to time in the exponential term in (11) and set it to zero. We find that

$$t_{st} = \frac{\sqrt{R_t} \gamma_p^2 X_p - \sqrt{R_p} \gamma_t^2 X_t}{v_p \left(\sqrt{R_t} \gamma_p^2 - \sqrt{R_p} \gamma_t^2 \right)} \quad (12)$$

which is the time of the stationary phase.

In the phase component of (11), we leave out $\frac{i4\pi f_c}{c}$ in the coming derivations and try to simplify it after inserting $t = t_{st}$ from (12). To start with, we apply the law of conjugates on the expression and obtain

$$\begin{aligned} \delta R(t_{st}) &= R_t(t_{st}) - R_p(t_{st}) \\ &= \frac{\gamma_t^2 (v_p t_{st} - X_t)^2 + Y_t^2 - \gamma_p^2 (v_p t_{st} - X_p)^2 - Y_p^2}{R_t + R_p} \end{aligned} \quad (13)$$

Now, using the fact from (12) that

$$v_p \tau_{st} - X_p = \frac{\gamma_p^2 \sqrt{R_p}}{\gamma_p^2 \sqrt{R_t}} (v_p t_{st} - X_t) \quad (14)$$

we obtain

$$\delta R(t_{st}) = \frac{\frac{\gamma_p^2 \gamma_t^2}{\gamma_p^2 - \gamma_t^2} \sqrt{\frac{R_p}{R_t}} (X_p - X_t)^2 + Y_t^2 - Y_p^2}{R_t + R_p} \quad (15)$$

Thus, we can write the final expression for the phase in the SAR image by multiplying with $\frac{4\pi}{\lambda_c}$ in (15) as

$$\theta(X_p, Y_p) = 4\pi \frac{\frac{\gamma_p^2 \gamma_t^2}{\gamma_p^2 - \gamma_t^2} \sqrt{\frac{R_p}{R_t}} (X_p - X_t)^2 + Y_t^2 - Y_p^2}{\lambda_c (R_t + R_p)} \quad (16)$$

IV. ESTIMATION PROCEDURE

The phase in (16) indicates that the phase in azimuth can be described as a quadratic function. By estimating this quadratic term we can find $\hat{\gamma}_t$. Therefore, we assume the following model for the phase in the SAR image in the azimuth direction:

$$\theta(X_p) = a_0 X_p^2 + a_1 X_p + a_2 + n_c(X_p) + n_0(X_p) \quad (17)$$

where $n_c(X_p)$ is a phase component from clutter and $n_0(X_p)$ is the phase component from noise generated by the SAR imaging algorithm along with receiver noise.

We now sample the phase of a range bin, $\theta_{p,s}$, in the given SAR image. This range bin in the SAR image is denoted by $S(X_p)$.

$$\theta_{p,s} = \text{atan} \frac{\text{Im}(S(X_p))}{\text{Re}(S(X_p))} \quad (18)$$

The amount of pixels used is experimentally decided. In this paper all pixels within the 3dB width were used. Having extracted these pixels, we can find the second derivative of this sequence by

$$\ddot{\theta}_{p,s} = \Delta_{X_p}^2 \theta_{p,s} \quad (19)$$

where $\Delta_{X_p}^2$ is the finite difference operator [19].

We suggest that the same estimator for the chirp rate as proposed in [19] and [16] is used, namely a BLUE estimator. The estimate is then

$$\hat{a}_0 = \frac{\mathbf{1}^T \mathbf{C}^{-1} \ddot{\theta}_{p,s}}{\mathbf{1}^T \mathbf{C}^{-1} \mathbf{1}} \quad (20)$$

where \mathbf{C} is the covariance matrix of the second derivative of the phase from $n_c(X_p)$ and $n_0(X_p)$.

By obtaining an estimate of a_0 , we can estimate γ_t .

The relation between a_0 and γ_t found from (16) is

$$\gamma_t = \left(\frac{8\pi}{\lambda_c(R_t + R_p) \hat{a}_0} + \frac{\sqrt{R_p}}{\gamma_p^2 \sqrt{R_t}} \right)^{-\frac{1}{2}} \quad (21)$$

In [20], a moving target and a stationary scatter were placed at the same position in the SAR image and the estimation accuracy was investigated by comparing if \mathbf{C} was based on the contributions from n_c and n_0 or only on n_0 . The results did not indicate any difference between the two cases unless in a special case when the image was formed for $\gamma_p = 1$. For this reason as well as for the sake of simplicity, \mathbf{C} will in this paper be used in its simplest form, namely based on a white noise approximation.

V. REFOCUSING IN A SAR IMAGE

In a way similar to that in [17], the idea is to refocus the moving target based on a SAR image. In this case however, the image needs not have been formed for $\gamma_p = 1$, but could have been created using arbitrary relative speed within the limits $0 < |v_{rel}| < 2|v_{pl}|$. In this paper, we propose a modified RMA, where the refocusing is applied in the wavenumber domain using a reinterpolation to the image plane. Range migration can be described by the change of variable

$$k_{\rho_{stat}} = \sqrt{k_R^2 - k_x^2} \quad (22)$$

where k_R is the range wave number, $k_{\rho_{stat}}$ is the slant-range wavenumber when focusing a stationary ground, i.e. $\gamma_p = 1$, and k_x is the azimuth wavenumber. If instead a moving target is to be focused, the azimuth wavenumber needs to be rescaled with the NRS of that moving target, corresponding to

$$k_{\rho_{MT}} = \sqrt{k_R^2 - \gamma_t^2 k_x^2} \quad (23)$$

However, if the original image is processed at an arbitrary NRS γ_p , the slant range wavenumber for that speed will be

$$k_{\rho_{stat}} = \sqrt{k_R^2 - \gamma_p^2 k_x^2} \quad (24)$$

and all moving targets with the NRS γ_p will be focused. If there is a moving target with $\gamma_t \neq \gamma_p$, that target will not be focused. However, if we first select an area surrounding the moving target in the image processed at γ_p and then transform this subimage to the wave domain and compensate by

$$k_{\rho_{MT}} = \sqrt{k_{\rho_{stat}}^2 + k_x^2 (\gamma_p^2 - \gamma_t^2)} \quad (25)$$

the moving target will be focused. This formula is found by inserting (24) in (23).

After this change of variable, the signal is multiplied with (26) and after an 2D inverse Fourier transform, a refocused SAR image at γ_t from an image focused at γ_p is obtained according to

$$\frac{k_{\rho_{stat}} e^{-j r_0} \left| \sqrt{(\gamma_p^2 - \gamma_t^2) k_x^2 + k_{\rho_{stat}}^2} \right|^{-k_{\rho_{stat}}}}{\sqrt{k_{\rho_{stat}}^2 + k_x^2 (\gamma_p^2 - \gamma_t^2)}} \quad (26)$$

VI. SIMULATION RESULTS

In this section, we present simulation results that illustrate how speed estimation can be estimated and a moving target refocused using the approach outlined above. The simulations are based on parameters chosen for a low frequency system, on an airborne platform at a distance close to the imaged scene, leading to a large integration angle even at short integration times. In Table I and Table II, the parameters for the simulation is given.

TABLE I
SIMULATION PARAMETERS

Parameter	Value
Center Frequency	350Mhz
Integration Time	20sec
Bandwidth	300Mhz
Minimum Range	1412m

TABLE II
TARGET PARAMETERS

Target	$v_x[m/s]$	$v_y[m/s]$	γ_t	$x_0[m]$	$y_0[m]$
A	4	0	0.9689	1288	925
B	1	0	0.9922	1288	975
C	5	-2	0.9613	1288	1000
D	2	0	0.9845	1288	1000
E	-4	0	1.0311	1288	1025
F	-2	0	1.0155	1288	1050

TABLE III
SIMULATION RESULTS

Target	$\hat{\gamma}_t$	γ_t	δ_{γ_t}
A	0.9673	0.9689	0.0016
B	0.9922	0.9922	0.0000
C	0.9586	0.9613	0.0027
D	0.9841	0.9845	0.0004
E	1.0290	1.0311	0.0021
F	1.0150	1.0155	0.0005

For the simulation, six targets with different speeds were chosen. The speeds of the targets are given in Table II. Based on the originally obtained image, Fig. 4, the signatures for each target are extracted, thus producing 6 smaller images. For each of these images, the estimation procedure in section IV was used to obtain an NRS estimate. The images were then refocused according to the procedure presented in the section V. In these new refocused images, new estimates are obtained and the images are yet again refocused. For each of the targets, up to three iterations are made. After this, the small focused images of the targets produced by the process are combined and the final result is obtained which is shown in Fig. 5. In Table III, the final NRS estimates obtained for all targets are shown, as well as the errors denoted δ_{γ_t} for each of the targets. The errors are larger

for the targets having larger $|1 - \gamma_t|$, thus leading to longer convergence times.

VII. REAL DATA RESULTS

To indicate the performance when using real data, a simulated moving target was inserted into a real SAR image obtained by the CARABAS-II system. The average energy of the moving target was chosen to be 2.5dB above the average power of the clutter in Fig. 7. However, since the relative bandwidth and beam width of this system are extremely large, and because low frequencies are used, single clutter scatterers become separated. This leads to some pixels becoming strongly focused such as those belonging to the trees in this case, while the surrounding pixels have very low power. In this specific scene with large trees, each tree scatterer is stronger than the target and therefore the target is hidden in the forest to a great extent. Because of this, it is important to obtain a measure of the target radar cross section (RCS) in relation to the strongest clutter scatterer in the surroundings. For a typical tree in this scene, the peak power, which is a measure of scatterer RCS, was 7 times the peak power of the moving target. The scene with the moving target superimposed is shown in Fig. 6 and a zoomed in version is depicted in Fig. 7. As can be seen in 7, the average energy of the moving target is larger than that of the clutter, even though the peak amplitude is on a level similar to that of the clutter.

The pixels are extracted and the estimation scheme as suggested in Fig. 3, using (21) for estimation, is applied. The number of focusing iterations for the moving target was set to 3. As can be seen in Fig. 8 and Fig. 9, the moving target is focused after the 3 iterations and the energy of the surroundings in the subimage is strongly suppressed. In this experiment, the target had an NRS of 1.0155 and the estimate obtained after the third and

last iteration was 1.0150, giving an error of 0.0005. For a target moving purely in azimuth, this corresponds to a speed of 2 m/s, and an estimate of 1.93 m/s which gives a relative error of 3.5%. For a target moving purely in range, this corresponds to 22.76 m/s and an estimate of 22.39 m/s, which gives a relative error of 1.6%. The estimate is thus close to the true value of the target NRS, showing that even in the case where the simulated target is superimposed onto clutter that partly covers the signal, using the proposed approach appears to work.

VIII. CONCLUSIONS AND DISCUSSION

In this section the main conclusions drawn from this paper are explained and the factors that affect the performance of the approach are discussed.

A. Conclusions

In this paper, an approach for estimating relative speed and focusing moving targets is proposed. The estimation of relative speed is based on a chirp estimator that makes use of the target phase. Focusing is made in subimages where the SAR image is transformed to the wave domain and compensated according to the target speed and the processing speed of the SAR image. The estimation and the focusing is then combined in an iterative process. The approach is illustrated with the help of one simulation and one experiment where a simulated target is superimposed onto a complex SAR image. We can conclude that even when the peak of the moving target signal is at the same level as the peaks of the surrounding clutter, the target can be refocused successfully. The refocused target can also successfully be combined with the original SAR image, thus providing the end user with good information on where the target was located in relation to the surroundings as well as the magnitude of its NRS. To conclude, we can say that the simulated and

real results show that the proposed approach to estimate and refocus appears to be functional.

B. Discussion

In order to obtain good results, the platform should preferably be located close to the imaged scene. The reason is that for shorter integration times, the dynamics parameters change less for moving targets. Another advantage is that this allows the platform to fly at a lower speed, allowing for higher accuracy when conducting the speed measurement since the accuracy of the actual speed measurement is related to the ratio between the target speed and the platform speed. It should be noted, however, that the method does not depend on these parameters, it only performs better when they are in place.

REFERENCES

- [1] D.J. Weydahl, C. Brekke, P. Selvik, Ø. Hellenen, and R. Olsen, "Ship traffic monitoring using satellite SAR images in combination with AIS reports" In Proceedings of SPIE Remote Sensing for Environmental Monitoring, GIS Applications, and Geology VII, Florence, Italy, 2007.
- [2] S.V. Baumgartner and G. Krieger, "SAR traffic monitoring using time-frequency analysis for detection and parameter estimation" In Proceedings of IGARSS, Boston, USA, 2008.
- [3] P. Meisl, A.A. Thompson, P.A. Luscombe, "RADARSAT-2 mission - overview and development status" In Proceedings of the 3rd European Conference on Synthetic Aperture Radar, Munich, Germany, 2000.
- [4] S. Buckreuss, W. Balzer, P. Mühlbauer, R. Werninghaus, W. Pitz, "The TerraSAR-X satellite project" In Proceedings of IGARSS, Toulouse, France, 2003.
- [5] R. K. Raney, H. Runge, R. Bamler, I. G. Cumming, and F. H. Wong, "Precision SAR processing using chirp scaling" IEEE Transactions on Geoscience and Remote Sensing, vol. 32, 1994.
- [6] C. Cafforio, C. Prati, and F. Rocca, "SAR data focusing using seismic migration techniques" IEEE Transactions on Aerospace and Electronic Systems, vol. 27, 1991.
- [7] L.E. Andersson, "On the determination of a function from spherical averages" SIAM Journal on Mathematical Analysis, vol. 19, 1988.
- [8] L. M. H. Ulander, M. Lundberg, W. Pierson, and A. Gustavsson, "Change detection for low-frequency SAR ground surveillance" IEE Proceedings on Radar Sonar and Navigation, vol. 152, 2005.
- [9] S. Axelsson, "Position correction of moving targets in SAR-Imagery" In Proceedings of SPIE - The International Society for Optical Engineering, vol. 5236, 2004.
- [10] C.H. Gierull, "Ground moving target parameter estimation for two-channel SAR" IEE Proceedings on Radar Sonar and Navigation, vol. 153, 2006.
- [11] P.A.C. Marques and J.M.B. Dias, "Velocity estimation of fast moving targets using a single SAR Sensor" IEEE Transactions on Aerospace and Electronic Systems, vol. 41, 2005.
- [12] V.T. Vu, T.K. Sjögren, M.I. Pettersson, H.-J. Zepernick and A. Gustavsson, "Experimental results on moving targets detection by focusing in UWB low frequency SAR" In Proceedings of IET International Radar Conference, Edinburgh, UK: 2007.
- [13] S. Barbarossa and A. Farina, "Detection and imaging of moving targets with synthetic aperture radar. 2. Joint time-frequency analysis by Wigner-Ville distribution" IEE Proceedings in Radar and Signal Processing, 1992.
- [14] F. Zhou, R. Wu, M. Xing, and Z. Bao, "Approach for single channel SAR ground moving target imaging and parameter estimation" IET Radar, Sonar and Navigation, vol. 1, 2007.
- [15] H. Zhou, X. Huang, Y. Chang, Z. Zhou, "Single-channel UWB SAR ground moving targets detection method using change detection based on single-pass sub-aperture images" In Proceedings of Asian Pacific Conference on SAR, Huangshan, China: 2007.
- [16] T.K.Sjögren, V.T.Vu and M.I.Pettersson, H.-J. Zepernick, A. Gustavsson, "Speed estimation experiments for ground moving targets in low frequency UWB SAR" In Proceedings for IET International Radar Conference, Edinburgh, UK: 2007.
- [17] J.K.Jao, "Theory of synthetic aperture radar imaging of a moving target" IEEE Transactions on Geoscience and Remote Sensing, vol. 39, September 2001.
- [18] M.I.Pettersson, "Detection of moving targets in wideband SAR" IEEE Transactions on Aerospace and Electronic Systems, vol. 40, July 2004.
- [19] P.M. Djuric and S.M. Kay, "Parameter estimation of chirp signals" IEEE Transactions on Acoustics, Speech and Signal Processing, vol. 38, 1990.
- [20] T.K.Sjögren, V.T.Vu and M.I.Pettersson, "Moving target relative speed estimation in the presence of strong stationary surrounding using a single antenna UWB SAR system" In Proceedings of IGARSS, Boston, USA, 2008.

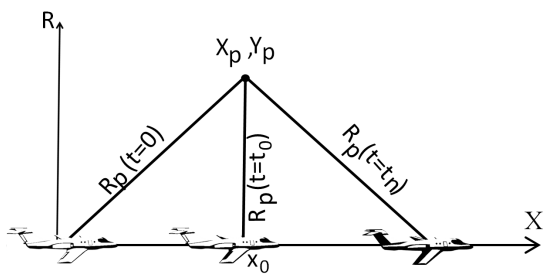


Fig. 1. SAR image formation geometry in cylindrical coordinates with respect to an arbitrary pixel.

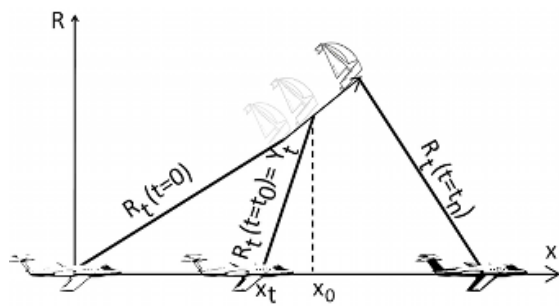


Fig. 2. SAR image formation geometry in cylindrical coordinates with respect to a moving target.

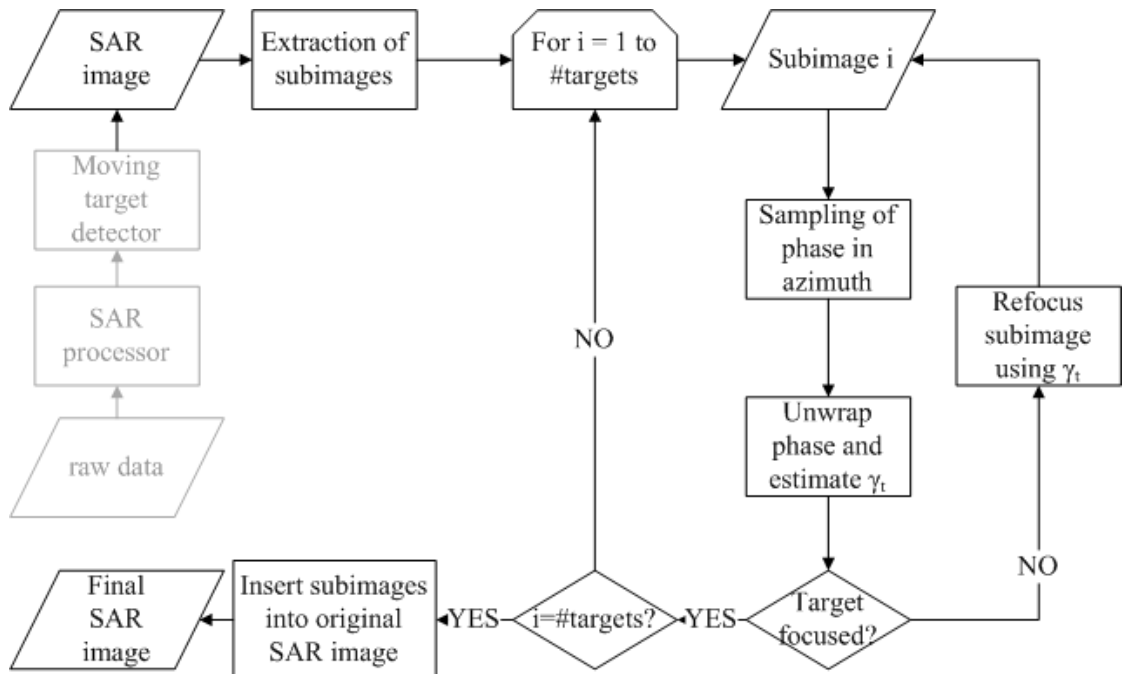


Fig. 3. Schematic sketch illustrating how the estimation and refocusing approach is applied.

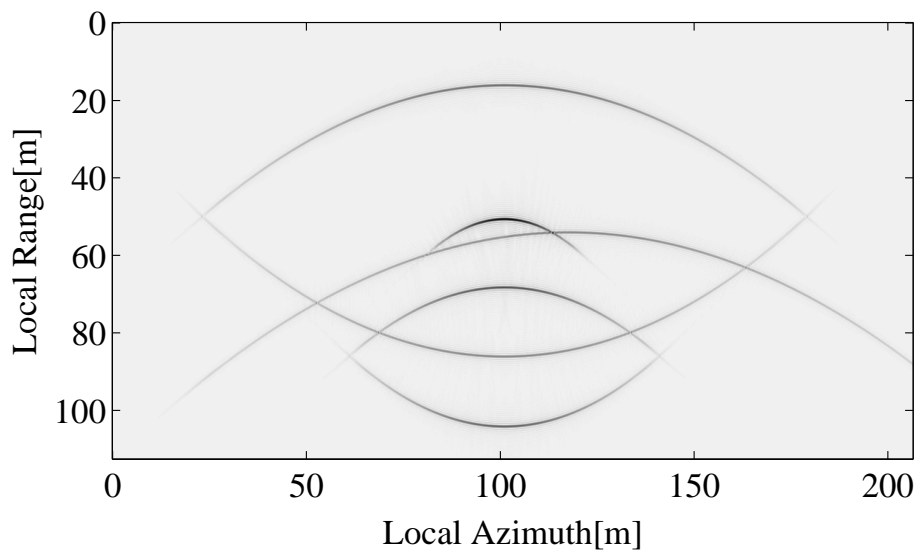


Fig. 4. Original simulated SAR image.

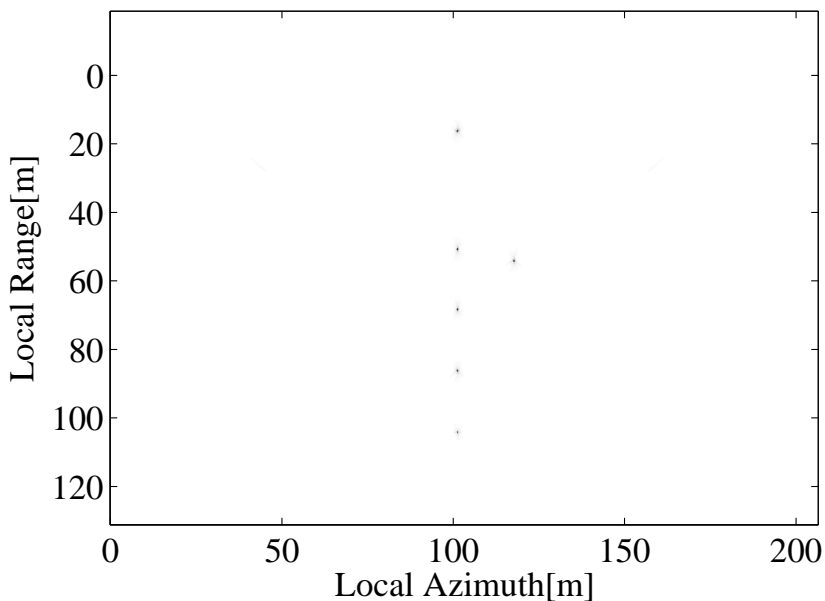


Fig. 5. Final image after iterative focusing of all targets seen in Fig. 4 and composition of respective subimages.

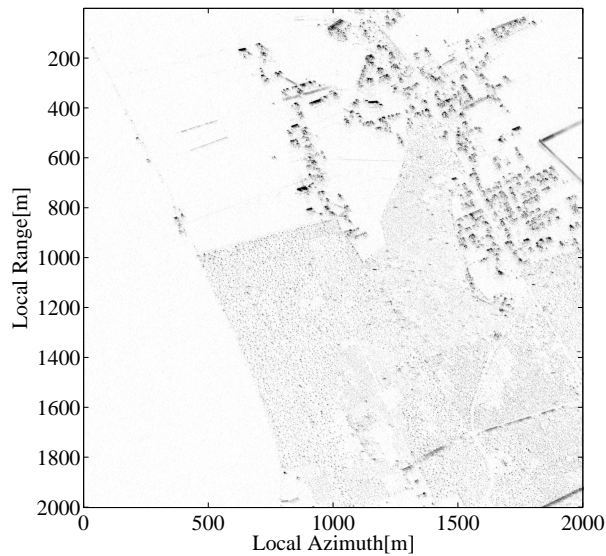


Fig. 6. SAR image of Visingsö where a simulated moving target has been synthetized and placed in the forest.

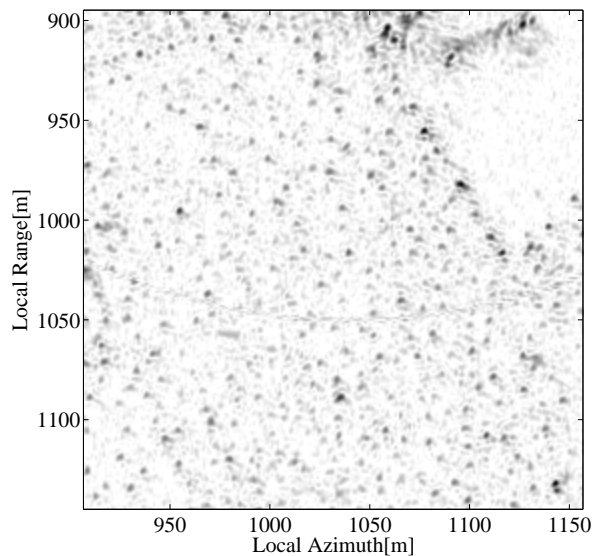


Fig. 7. A zoom in of the simulated moving target which has been added to the SAR scene.

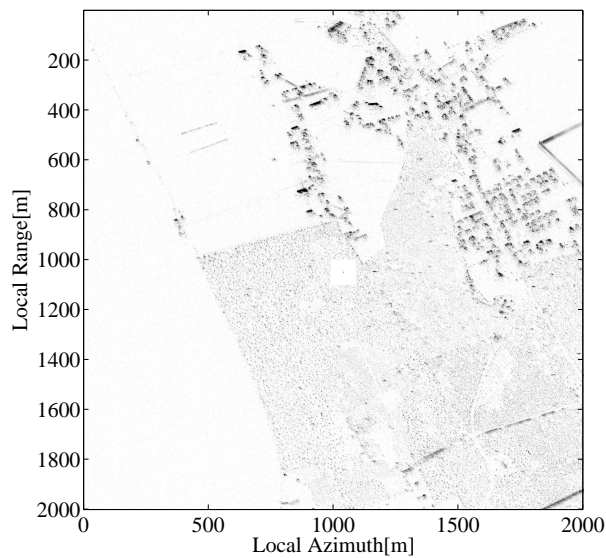


Fig. 8. Final SAR image after iterative focusing and combination with original SAR image.

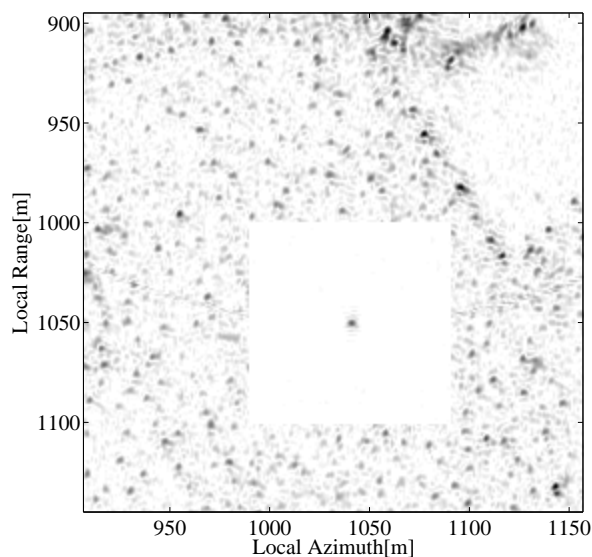


Fig. 9. Zoom in of the focused moving target.